Chapter 11

Dancing angels on the point of a needle: nanofabrication for subwavelength optics

Mikhail Y. Shalaginov[1], Fan Yang[1], Juejun Hu[1] and Tian Gu[1,2]

11.1 Opening remarks

The point of a needle is often used as a metaphor for miniscule objects and has hence inspired the classical question: How many angels can dance on the point of a needle? In the emerging world of nanotechnology, however, there is a plenty of room on the point of a needle and it can easily be a dancing stage for engineers equipped with state-of-the-art nanofabrication tools (literally—as we shall show later).

In optics, the capability to produce and manipulate nanoscale structures has culminated in subwavelength optics that provide unprecedented control over light propagation compared to their traditional bulk or wavelength-sized counterparts. Other chapters of this book have unveiled the fundamental theory as well as the fascinating prospect of leveraging subwavelength nanoantennas and nanoplasmonic structures for light manipulation. In this chapter, we will focus on the technologies that are used to create subwavelength optical devices. Since there are already a number of well-written textbooks and review articles describing nanofabrication methods in general [1–5], we feel that repeating another exhaustive review about nanofabrication offers little value to the community. Instead, here we choose to highlight the difficulties associated with subwavelength structure processing and give a snapshot of the ingenious solutions that have been developed to tackle these challenges.

Compared to processing of semiconductor nanoelectronics, subwavelength optics fabrication is unique in two ways. First, nanofabrication of subwavelength optics often involves a wide range of materials not necessarily within the repertoire of standard Complementary Metal-Oxide-Semiconductor (CMOS) processing to achieve desired optical functions. The examples include noble metals for plasmonics, transparent

[1]Department of Materials Science & Engineering, Massachusetts Institute of Technology, Cambridge, MA, USA
[2]Materials Research Laboratory, Massachusetts Institute of Technology, Cambridge, MA, USA

conducting oxides for active photonics, and chalcogenide compounds for high-index-contrast metasurfaces. Second, even when only standard materials are utilized, the fabrication processes often have to be customized to meet the unique requirements set forth by optical applications: fabrication of metasurfaces operating in the visible spectrum based on high-aspect-ratio (HAR) TiO_2 nanostructures is a case in point [6]. In light of these unique features, the remainder of this chapter is organized into two sections. We will start by evaluating various material platforms and standard planar nanofabrication methods in the context of subwavelength optical structure definition. The second part of the chapter covers strategies to realize three classes of structures that often present significant fabrication challenges to experimentalists, yet are highly relevant for subwavelength optics: HAR structures, 3D components, and devices on unconventional, non-planar substrates.

11.2 Standard planar nanofabrication technologies applied to subwavelength optics

Subwavelength optics deals with artificial optical interfaces that provide on-demand control of phase, amplitude, and polarization of light, a capability not available in natural materials. By arranging nanostructured optical elements in flat subwavelength arrays, planar subwavelength optics (such as metasurfaces) can leverage standard nanofabrication techniques for potential low-cost, scalable manufacturing [5,7–20]. In addition to material property and process optimization, key considerations for fabricating such nanostructures include resolution, precision, reproducibility, throughput, reliability, cost effectiveness, and CMOS compatibility. With the development of the semiconductor industry, current lithographic fabrication techniques nowadays offer high resolution, complex geometry definition, high throughput, and high reproducibility for manufacturing planar nanoparticles. In order to achieve desired optical functionalities at the subwavelength scale, non-traditional materials or customized processes are usually needed. In this section, traditional planar nanofabrication approaches adapted for fabricating planar subwavelength optics are reviewed and discussed. Additionally, prospects for scaled-up manufacturing which leverages available tools from the semiconductor industry are further discussed.

11.2.1 Materials for subwavelength optics

11.2.1.1 Plasmonic subwavelength optics

Subwavelength optics has been initially based on metallic nanoparticles made of noble metals (e.g., gold and silver) to enhance light concentration at the nanoscale, which, in turn, enables versatile manipulation of electromagnetic waves [21–25]. Among metals, gold and silver exhibit lower loss in the visible and near-infrared spectral range. Both of them can be deposited using physical vapor deposition techniques, such as electron beam evaporation, thermal evaporation, or sputtering. A typical method for patterning metallic nanoparticles involves electron beam lithography (EBL) to define the structures. As shown in an exemplary fabrication

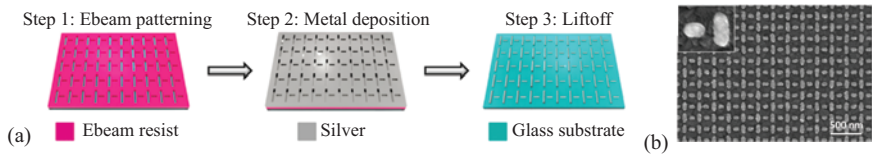

Figure 11.1 Typical fabrication flow of a plasmonic metasurface [25].

process flow in Figure 11.1 [25], a substrate is first coated with an electron beam resist layer, and subsequently exposed and patterned by a scanning focused electron beam. After development of the resist, a metal layer is deposited and patterned on the substrate via liftoff. Multiple metallic layers can be integrated in stacks to allow individual tuning of the induced radiation coming from both sides of the meta-device [16,26–28]. This enables, for example, plasmonic metasurface designs combining resonant phase tuning and the Pancharatnam–Berry (PB) phase.

The excessive losses of metals have severely limited the device performance at optical frequencies. Potential alternative plasmonic materials have been explored [29,30], such as transparent conducting oxides (TCOs) [30], intermetallics (e.g., silicides, germanides, borides, and nitrides) [31], metallic alloys [32], graphene [33], etc. In particular, TCOs have been widely used in optoelectronic devices with well-developed CMOS-compatible processes. When employed in nanophotonics, TCO nanostructures based on ITO, ICO, or ZnO doped with Al or Ga allow tailorable device functionalities [34–38]. For instance, ITO is a potential candidate for plasmonic materials operating in NIR [39,40]. Due to its non-stoichiometric nature, the material deposition process and annealing conditions can play major roles in determining the material optical performance. High-quality ITO films can be produced by sputtering or laser ablation [41]. Significant variance of dielectric functions have been observed when ITO films were annealed at different conditions, including both annealing temperature and ambient gas environment [30,42].

Al- or Ga-doped ZnO films can also be deposited by sputtering or laser ablation. The deposition conditions (temperature and oxygen partial pressure) and dopant concentration are important to obtain low-loss, high-quality films [30,43,44]. In one example, TCO metasurfaces made of Ga:ZnO were developed and used as a quarter-wave plate (QWP) for polarization control in the NIR spectral region [45]. The metasurface consisted of orthogonally patterned nanorod arrays designed to provide a phase difference of $\pi/2$ for perpendicularly polarized light. As schematically depicted in Figure 11.2, the Ga:ZnO film was deposited on a glass substrate using pulsed laser deposition. A dry-etching method with bilayer resists involving hydrogen silsesquioxane (HSQ) for masking and poly(methyl methacrylate) (PMMA) as the sacrificial layer was developed to fabricate the metasurface. Owing to Ga:ZnO's weak dispersion of dielectric function, a broadband QWP functionality was realized.

11.2.1.2 Silicon-based materials

Plasmonic subwavelength optics are inherently restricted by the large Joule losses. They typically operate in the reflection mode, which further restricts the application

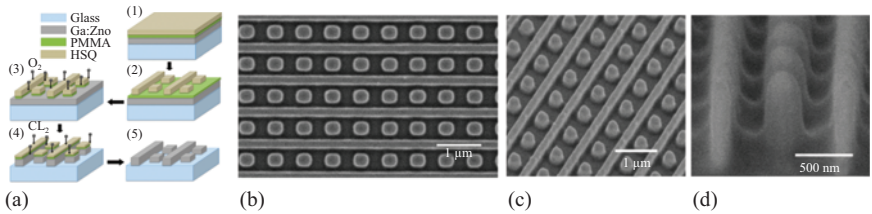

Figure 11.2 (a) Process flow for fabrication of Ga:ZnO metasurfaces using reactive-ion etching (RIE) with bilayer resist. (1) Spin-coating of PMMA and HSQ layer over Ga:ZnO film, (2) e-beam lithography of HSQ resist, (3) O_2 RIE etch of PMMA with HSQ as the etch mask, (4) CL_2 (which stands for chlorine) RIE etch of Ga:ZnO with HSQ and PMMA as the etch mask, and (5) removal of PMMA and HSQ etch mask with acetone. (b) Top view, (c) 30° tilted view, and (d) cross-sectional (75° tilted) view of the FESEM image of a fabricated Ga:ZnO metasurface [45].

space. All-dielectric nanoparticles can eliminate such unfavorable aspects and enable a large array of meta-optics with performance comparable to commercial bulk optical components [46–49]. Such high-index nanoparticles support high-quality Mie resonances and low-profile nanostructure designs [5,49]. The low optical loss, enhanced electric and magnetic resonances, tunability of scattering directionality, and CMOS compatibility make all-dielectric metasurfaces a desirable platform to realize high-performance flat optical devices with scalable manufacturing capability. Here, we review planar nanofabrication techniques adopted for fabricating dielectric metasurfaces.

The utilization of silicon in subwavelength optics has been investigated extensively owing to several beneficial properties, such as high refractive index and low absorption loss within telecommunication wavelengths [50], as well as strong electric and magnetic multipolar responses associated with Si nanoparticles. Furthermore, Si is the backbone of state-of-the-art electronic and photonic technologies, offering compatibility with standard CMOS processes.

Silicon-based subwavelength nanostructures can be fabricated using lithographic methods, which provide precise control of the optical responses with a variety of nanoparticle geometries [51–53]. Typical process steps based on EBL for fabricating silicon-based nanoparticles are schematically illustrated in Figure 11.3(a) [12]. Monocrystalline silicon-on-insulator wafers or low-index substrates (such as quartz) coated with amorphous or polycrystalline silicon films deposited via low-pressure chemical vapor deposition (LPCVD) or plasma-enhanced chemical vapor deposition (PECVD) are typically used. The film is then patterned by EBL and reactive-ion etching (RIE). Examples of fabricated silicon nanodisk structures are shown in Figures 11.3(b) and (c).

Functional meta-optic devices further require the integration of multiple metasurfaces, optical apertures, and stops, as well as alignment features to form an

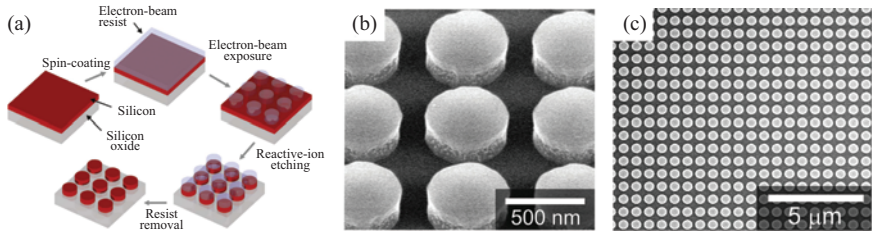

Figure 11.3 *(a) Typical process steps for fabricating high-index dielectric subwavelength nanoparticles using e-beam lithography [12]; (b) and (c) scanning electron micrographs of fabricated silicon nanodisks [51].*

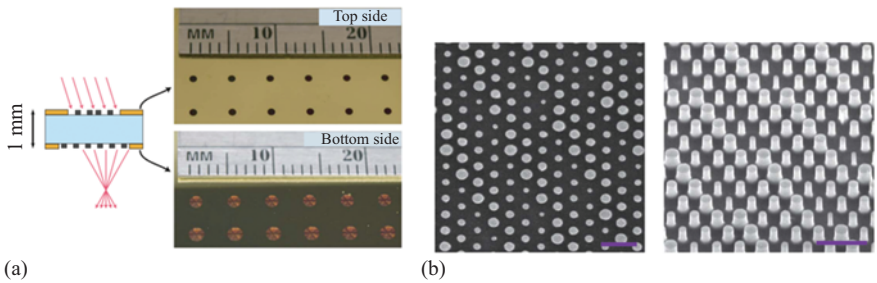

Figure 11.4 *(a) Schematic and optical images of a doublet metalens consisting of two metasurfaces formed on both sides of a fused silica substrate. (b) SEM images of fabricated metasurfaces consisting of a-Si nanoposts [54]. Scale bars, 1 μm.*

optical system. Along this direction, a doublet lens with metasurfaces fabricated on both sides of a fused silica substrate was demonstrated, as shown in Figure 11.4 [54]. Hydrogenated amorphous Si (a-Si) layers were deposited on both sides of the substrate via PECVD and defined into nanopost patterns via EBL and dry etching. After the first metasurface was patterned on one side of the substrate, the second metasurface was lithographically aligned and patterned on the other side. The patterned side of the substrate is protected by a polymer layer while the other side is being processed. Apertures were created by patterning opaque metal layers on both sides of the wafer, followed by coating of antireflection layers.

It is also possible to fabricate metasurfaces on membranes to take advantage of their nanoscale flat architecture. A MEMS-actuated dielectric metalens was demonstrated consisting of a movable metasurface on a silicon nitride membrane and a fixed metasurface on a glass substrate. The distance between the two metasurfaces was controlled by electrostatic actuation of the membrane [53]. To fabricate such a movable metasurface, a SiO_2 layer was first deposited on a SiN coated

Si wafer, followed by the deposition of an a-Si layer. After the metasurface was patterned into the a-Si layer and metal contacts were defined, the remaining part of the wafer under the membrane was removed via wet etching. Then, the metasurface was released after the membrane was patterned and dry etched. To provide alignment between the front and back sides of the a-Si layer, alignment marks were etched through the layer.

In [55], substrate conformal soft-imprint lithography was combined with RIE to fabricate silicon nanocylinders used as subwavelength Mie resonators, which provided efficient broadband omnidirectional antireflection coatings on a silicon wafer. The soft-imprint lithography process employed a PDMS stamp molded from a master Si wafer to replicate patterns onto a sol–gel layer spin-coated on the target Si wafer. RIE was subsequently utilized to define Si nanoparticles using the sol–gel patterns as a mask. By coating the silicon nanocylinders with an additional Si_3N_4 coating using LPCVD, the reflection reduction was further enhanced.

Silicon nitride (SiN) possesses a broadband transparency ranging from near UV to infrared and is compatible with CMOS processes allowing integration leveraging existing foundry infrastructures [53,56–58]. A low-contrast dielectric metasurface based on SiN was demonstrated in [58]. The authors designed and fabricated vortex beam generators using SiN operating in the visible spectral range, leveraging low visible absorption of SiN and CMOS compatibility of the material.

11.2.1.3 III–V-based materials

III–V semiconductors (such as GaAs, GaN, and GaP) are of great interest to subwavelength optics due to their high refractive indices and excellent optoelectronic properties [59–64]. In particular, GaAs nanoparticles with zero optical backscattering have been demonstrated using a hybrid integration process [63]. As shown in Figure 11.5(a)–(c), epitaxial liftoff was utilized to transfer a 1 μm-thick GaAs membrane onto a fused silica substrate. The film was then thinned by RIE and patterned into nanostructure arrays with EBL and RIE. Furthermore, multistep lithographic processes for creating GaAs metasurfaces were developed based on selective wet oxidation (Figure 11.5(d)–(f)) [60–62]. Here, HAR etching was performed along with selective wet oxidation of AlGaAs underlayers to fabricate GaAs metasurfaces. As a result, multilayer GaAs metamaterials were realized with an embedded low-index native oxide layer between the nanoresonators and the substrate designed for broadband high reflectivity. In another example [62], the fabrication process began with epitaxial growth using MOCVD or MBE. This was followed by e-beam lithography and ICP dry etch to pattern the etch masks. Subsequently, the selective wet oxidization of AlGaAs was performed to form $(Al_xGa_{1-x})_2O_3$.

11.2.1.4 Chalcogenide compounds

Chalcogenide alloys, compounds containing one or multiple chalcogen elements (e.g., sulfur (S), selenium (Se), and tellurium (Te)), are attractive candidates for building subwavelength IR optics, owing to their exceptional optical properties, such as broadband infrared transparency, large refractive indices, tailorable

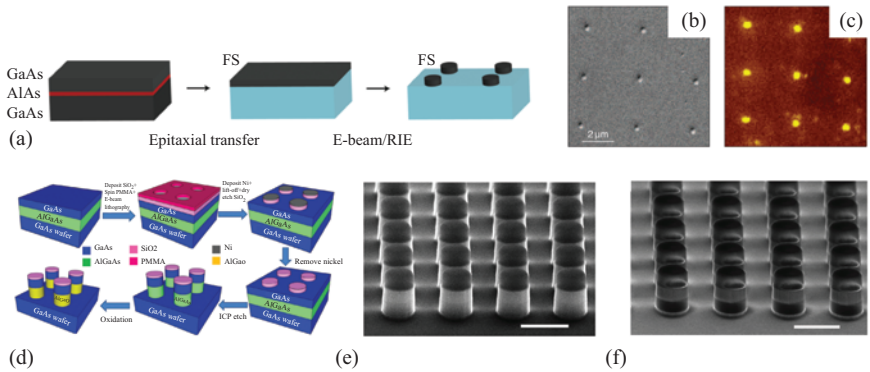

Figure 11.5 *(a) Fabrication process of GaAs nanopillars and (b) SEM image of GaAs nanopillar arrays (radius ∼ 90 nm). (c) Confocal photoluminescence image of the nanopillar arrays [63]. (d) Fabrication process for constructing AlGaAs-based dielectric metasurfaces. SEM images showing GaAs dielectric nanocylinders (e) before and (f) after the selective wet oxidation process. The scale bar corresponds to 1 μm [62].*

optical properties, large optical nonlinearity, and versatile fabrication processes with epitaxy-free deposition of high-quality thin films [65–70]. Furthermore, chalcogenide-based phase-change materials (PCMs) undergo dramatic, nonvolatile electrical and optical property change between their amorphous and crystalline states under external thermal, optical, or electrical stimuli, qualifying them as promising materials enabling active reconfigurable photonics [71].

Tellurium dielectric metamaterials and metasurfaces have been developed [72–74]. Te nanocubes have been fabricated on a barium fluoride (BaF_2) substrate and designed to center the magnetic resonance reflection peak at 10 μm [72]. In this work, a 1.7-μm-thick Te film was deposited on a BaF_2 substrate using electron-beam evaporation, with the nanostructures patterned by EBL followed by RIE. A multi-cycle deposition-etch process was utilized to fabricate the Te dielectric metamaterial structures [74], as shown in Figure 11.6(a). The multiple cycles of the deposition-etching-liftoff process reduce the deposition thickness of Te each time and effectively mitigate pinch-off issues during deposition. The fabricated nanocubes are shown in Figure 11.6(b), in contrast to the structures fabricated from a single deposition/liftoff step (Figure 11.6(c)), which suffer from severe pinch-off effect resulting in tapered meta-atom geometry.

Besides Te, PbTe is another material boasting a high refractive index larger than 5. It is thus ideally suited for forming dielectric meta-atoms supporting high-quality Mie resonances [75,76]. By monolithically integrating a nanocrytalline PbTe thin film on a low-index CaF_2 substrate ($n = 1.4$) and utilizing a dielectric Huygens meta-atom design, high-efficiency mid-infrared (mid-IR) transmissive meta-optic devices have been demonstrated [76]. The combination of PbTe and

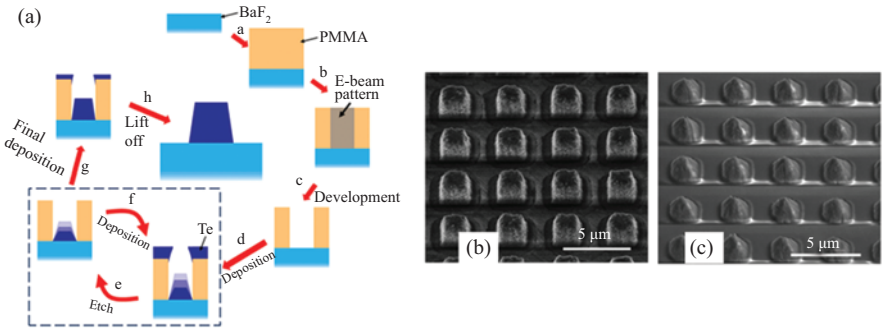

Figure 11.6 *(a) Multi-cycle deposition-etch process for patterning Te films; (b) Te dielectric metamaterial structure fabricated using multi-cycle deposition-etching-liftoff technique; (c) Te dielectric metamaterial structure fabricated using a single deposition-liftoff step [74].*

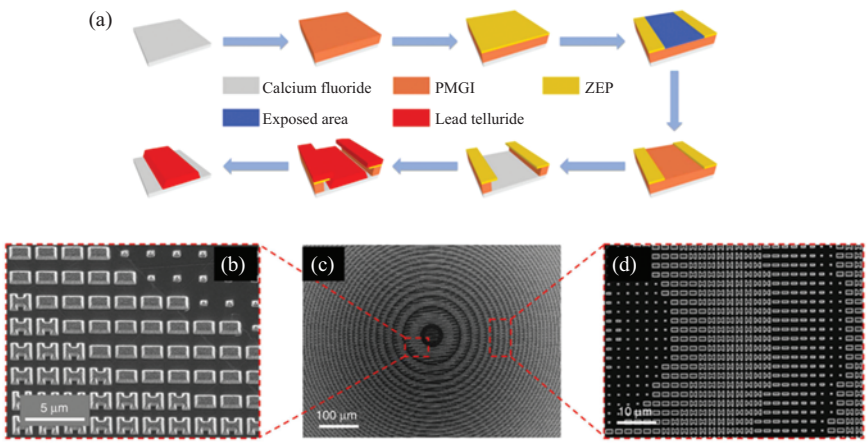

Figure 11.7 *(a) Schematic fabrication process flow of the meta-optical devices; (b)–(d) Top-view SEM micrographs of the fabricated aspheric metalens.*

CaF_2 contributes to an ultra-thin profile of the meta-atoms due to their large index contrast, with a thickness of only 1/8 of the operating wavelength in free-space (i.e., 650 nm at the 5.2 μm wavelength), as well as low optical attenuation from 4 to 9 μm wavelengths. The double-layer liftoff process and devices fabricated using this method are shown in Figure 11.7. This work marks the first experimental realization of a Huygens metasurface in the mid-IR and the first demonstration of diffraction-limited focusing in the mid-IR using transmissive metalenses. The material selection further foresees scalable manufacturing of meta-optics with large-area, high-throughput (growth rate ~100 nm/min) PbTe film deposition via

simple single-source thermal evaporation and wafer-scale lithographic patterning of the film [77–80].

11.2.1.5 Phase-change materials

Optical phase-change materials (O-PCMs) exhibit drastic optical property changes upon undergoing solid-state phase transformations [71]. Such transitions can be triggered by thermal, optical, or electrical stimuli and are attractive for photonic applications to realize reconfigurable optical devices. A subset of chalcogenide alloys possesses such phase-change properties, such as the commonly used GeSbTe (GST) alloy, a popular material for nonvolatile, tunable subwavelength optics [81–87]. In [81], GST films with a thickness of 70 nm were sputtered on a glass substrate coated with a ZnS–SiO_2 layer. After deposition of the GST film, a protective ZnS–SiO_2 layer is subsequently applied. Then, a reversible index modification from phase transition is induced optically by applying trains of femtosecond pulses onto the GST film (Figure 11.8(a)). As a result, reconfigurable flat optics with binary or grayscale patterns are created by using a diffraction-limited resolution optical writing process (Figure 11.8(b)–(f)).

Despite the large index modulation Δn of GST, they also exhibit considerable optical losses due to the relatively small bandgap and excessive free carrier absorption (FCA), limiting their optical performance as well as application space. Recently, a new group of O-PCMs, Ge–Sb–Se–Te (GSST), has been developed and implemented in integrated photonic and meta-optic devices [88]. GSST features

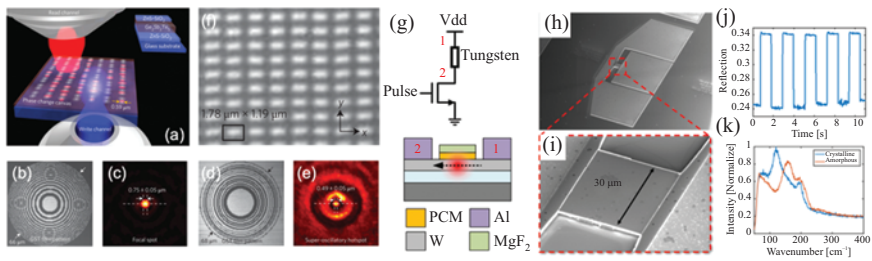

Figure 11.8 (a) Laser writing of reconfigurable photonic devices in GST phase-change film to locally vary the film property between its amorphous and crystalline states. (b) Fresnel zone plate written in phase-change film and (c) optical hotspot focused by this lens at 730 nm wavelength. (d) Binary super-oscillatory lens patterned in the phase-change film and (e) optical hotspot focused by this lens at 730 nm wavelength. (f) Dielectric metamaterials written in the phase-change film. (g) Schematic of electrothermal switching of GSS_4T_1. (h) SEM of the full device used to switch a 30 μm × 30 μm pixel. (i) Zoom-in on the pixel with a square pattern of GSS_4T_1. (j) Time-dependent absolute reflection measurements of a 1,550-nm laser focused onto the pixel. (k) Raman measurements of the GSS_4T_1 film after being triggered by amorphization and crystallization pulses.

unprecedented broadband optical transparency covering the telecommunication bands to the long-wave infrared (LWIR). Thin films of GSST can be deposited by thermal evaporation from a single $Ge_2Sb_2Se_4Te_1$ source and patterned using standard RIE or liftoff fabrication processes. Record low losses in nonvolatile photonic circuits and reconfigurable metasurfaces have been demonstrated. As an example, electrical pixelated switching of meta-optic devices was realized by integrating micro-heaters underneath thin-film GSST, as shown in Figure 11.8(g)–(i). Complete, reversible, and repeatable switching of the GSS_4T_1 film between its amorphous and crystalline states has been demonstrated (Figure 11.8(j) and (k)).

Another approach for constructing reconfigurable nanophotonic devices involves the integration of volatile phase-transition materials, such as vanadium dioxide (VO_2) [89–91], which also exhibit large optical property modification under external stimuli, albeit in a volatile way. The nanostructures were usually either directly patterned in VO_2 [90,92,93], or formed from plasmonic metals positioned on top of or embedded in a tunable VO_2 layer [90], [94–98]. In addition, the epitaxial growth of VO_2 on a sapphire substrate to form deep subwavelength VO_2 nanobeams was demonstrated [99]. This approach potentially allows fabrication of large-area tunable metasurfaces without resorting to nanostructuring processes.

11.2.1.6 2D van der Waals materials

2D materials (e.g., isolated single-layer graphene) are another attractive platform for subwavelength optics [7], [100–105]. Graphene exhibits highly variable dielectric permittivity useful for realizing active photonic devices. Nanostructures such as nanodisks, nanorods, and nanoholes have been demonstrated with broadband tunable resonances [101,106–108]. It also supports plasmonic resonance in the mid-IR spectral regime with high-quality factors and tight field confinement [101,102,109].

So far, the integration of 2D materials onto photonic devices typically employs layer transfer of exfoliated 2D membranes onto another substrate containing photonic devices [110]. This "hybrid" integration approach has been widely adopted but is limited by the topology of underlying structures or would require an additional planarization process to avoid rupture of the 2D membranes at structure corners [111,112]. Meanwhile, the interaction region between the optical mode and 2D layer is limited to the top of the optical structure. A monolithic integration approach is more desirable in terms of improving manufacturing yield, throughput, integration precision, and flexibility of device design. Such an approach would involve the growth of optical films on 2D materials and subsequent lithographic patterning of photonic devices [113–115]. However, it is not trivial to grow optically thick dielectric films on 2D materials due to its chemically inert surface, which makes nucleation and growth of uniform dielectric films challenging [116]. Surface modification could catalyze nucleation via ozone [117], NO_2 [118], or perylene tetracarboxylic acid [119], while sacrificing carrier mobility in graphene. While the former process tends to severely degrade graphene quality and the latter is not practical for growing optically thick layers, without the surface functionalization, continuous dielectric films could be formed via electron beam evaporation

or atomic layer deposition (ALD). PECVD is another potential alternative approach, while low-density, low-power plasma is required to mitigate plasma damage to graphene surface [120]. In general, the integration of 2D materials requires special attention on protecting the material's structural integrity from high temperatures, plasma, and reactive chemicals used during the process.

Amorphous chalcogenide glasses have recently been demonstrated as an ideal material candidate for integration with 2D materials. The glasses' amorphous nature and good van der Waals adhesion to different substrates allow epitaxy-free and substrate-agnostic deposition with minimal induced thermal and structural damages. Optically thick chalcogenide glass films have been deposited on a variety of 2D materials and patterned into functional optical devices without degrading the material and device properties [100]. Figure 11.9(a) schematically depicts a generic fabrication process to integrate chalcogenide glass photonic devices with graphene. Multi-layer photonic structures with 2D materials embedded inside optical structures were also realized, which optimized the interaction between the optical mode and 2D layer (Figure 11.9(b)).

11.2.2 Large-scale manufacturing: a case study of optical metasurfaces

Optical metasurfaces have revolutionized how optical components are designed and fabricated by completely deviating from the conventional operation principles

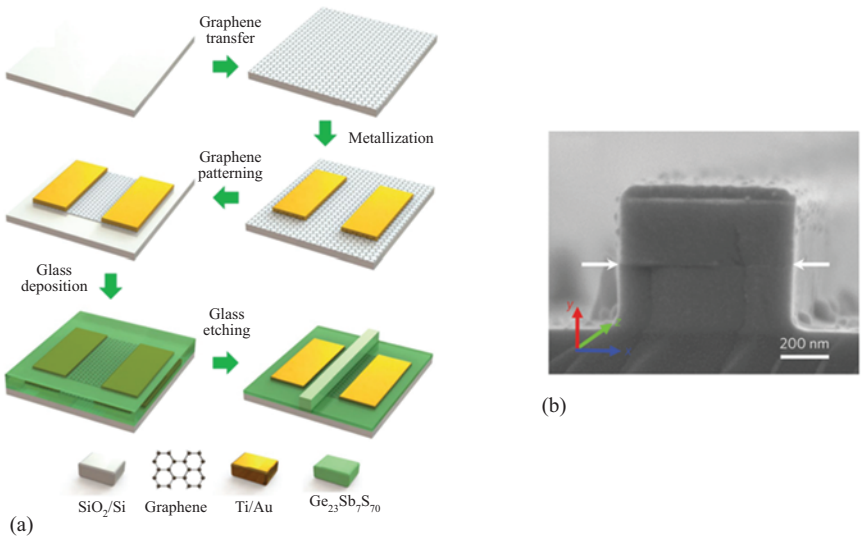

Figure 11.9 (a) Generic schematic fabrication process to integrate chalcogenide glass (ChG) photonic devices with graphene; (b) SEM image of the fabricated ChG waveguide structure embedding graphene; white arrows mark graphene location [100].

based on bulk optical materials. Instead, the wavefront of light is efficiently "molded" by a subwavelength array of nanostructures. Such an optically thin and planar architecture can potentially leverage microfabrication processes matured in the semiconductor industry to enable large-volume, low-cost, and scalable manufacturing. While EBL is a versatile fabrication tool widely used in the research community and well suited for prototyping purposes, the process is relatively costly and time consuming. For large-scale manufacturing, alternative high-throughput, low-cost fabrication approaches, such as photolithography, interference lithography, nanoimprinting, etc., are preferred. Meanwhile, wet etching processes can be utilized to potentially replace RIE processes for select applications [121].

Toward the goal of scalable fabrication, stepper lithography has been employed to fabricated large-area (a few centimeters in diameter) flat lenses based on metasurfaces with high yield [15]. The fabrication methodology and fabricated devices are shown in Figure 11.10. Here, an a-Si layer (600 nm thick) was first deposited on a 4-inch fused silica wafer using PECVD. After applying the photoresist and contrast-enhancement layers, the pattern of the metalens, which was carried out by a quartz photomask, was projected onto the wafer via an i-line stepper. After development, RIE was used to create the nanopost arrays in the a-Si layer. The use of a stepper allows the rapid replication of the metalens patterns over the entire wafer area by incrementally stepping the wafer position and repeating the exposure process, allowing the fabrication of hundreds of wafers per hour. Lastly, the wafer was diced into individual metalenses with diameters of 2 cm each. High-quality imaging performance has been achieved using the metalens fabricated via this approach.

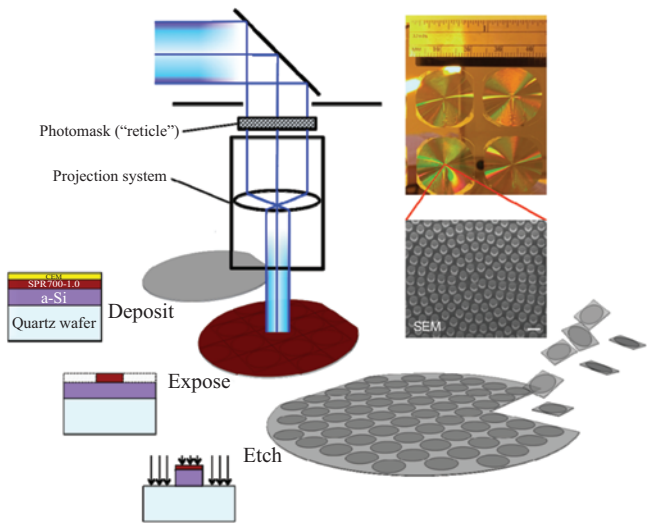

Figure 11.10 Schematic diagram of using photolithographic stepper technology for metalens fabrication over a 4-inch silicon wafer [15].

As the authors discussed in [15], one of the major challenges for scaled-up manufacturing of metasurfaces is the handling of very large metasurface layout files. To fulfill the subwavelength requirement, billions of meta-atoms with nanometer-scale precision are needed to fill the entire device aperture of a few centimeters in size, resulting in file sizes of hundreds of gigabytes. A multi-level compression algorithm taking advantage of rotational symmetry of metalens designs was thus developed to dramatically reduce the file size by several orders of magnitude [15]. Such an approach can be applied to other large-area fabrication methods for metasurfaces, such as nanoimprint and interference lithography.

Other challenges associated with fabricating large-area metasurfaces include local and global variance of the substrate over a large area, such as surface roughness, flatness, parallelism, etc. It should be noted that the impacts of these non-idealities are highly dependent on meta-atom design and meta-optic device architecture. For metalenses, variance of such parameters of commercial off-the-shelf wafers still guarantees good focusing and imaging performance at the expense of reduced optical efficiency, according to the analysis in [15]. For other types of devices (e.g., beam deflectors), however, such variance will enhance unwanted diffraction orders and result in cross-talks [76]. Thus, performance sensitivity to wafer parameter variances must be taken into account in the design phase with a thorough tolerance analysis.

11.3 Innovative solutions to nonconventional subwavelength optics designs

In the following sub-sections, we present the challenges and available solutions to the fabrication of three types of subwavelength optical structures: HAR structures, 3D structures, and devices on unconventional, non-planar substrates. Each sub-section begins by elaborating the significance of the type of structures and the unique optical functions they furnish. Various fabrication approaches are subsequently reviewed and compared.

11.3.1 HAR nanostructures

Advances in theoretical studies and numerical simulations of nanophotonic structures inspire scientists to further push the boundaries of fabrication capabilities. One of such avenues is to attain HAR nanostructures, which can enable significant improvements in imaging, sensing, energy harvesting, and secure communication. For instance, dielectric metalenses with HAR elements can achieve significantly higher focusing efficiencies and achromatic performance [64,122,123]; metamaterials and photonic crystals with narrow and deep trenches can support novel surface and bulk modes [124,125]; diamond nanowire-antenna arrays with color centers can unlock efficient on-chip single-photon generation [126]; ultra-narrow plasmonic gaps of <1 nm can lead to much stronger field enhancement, enabling quantum phenomena such as room-temperature strong coupling [127].

The scope of the developed techniques for achieving HAR structures is extremely broad, and the reader can refer to several reviews on the topic, for instance, the work by Lee *et al*. [128]. In this section, we would like to focus on several pattern transferring methods, which, in our opinion, are the most suitable for constructing high-quality subwavelength optical structures over large areas (mm-scale and larger) using commonly available cleanroom facilities. The quality of the HAR nano-optical devices is quantified by sidewall roughness ($<\lambda/100$), sidewall angle, and surface chemical contamination. Each of the following HAR techniques is presented below with a brief description of the technique and its principle of operation, general guidelines for achieving desired fabrication metrics, its advantages and limitations, as well as the state-of-the-art of fabricated devices.

11.3.1.1 Reactive-ion etching

Dry etching is an essential part of todays integrated circuit manufacturing line. Back in the early days of the semiconductor industry, wet etching was a dominant process used in pattern transfer processes. However, over the years wet etching was replaced with dry etching methods due to the necessity of reducing chemical waste and need to fabricate vertically standing elements with small feature sizes. One of the fascinating demonstrations of state-of-the-art etching technology are the 50:1 extremely HAR channels in a 3D flash memory stacks [129], known as the "Burj Khalifa towers" at the nanoscale.

RIE is the most common dry etching technique employed nowadays. In a RIE process, the material is selectively removed by a combination of chemical reaction and physical ion bombardment. The synergy between the two processes produces substantial increase in etching rates and selectivity [130]. RIE plasma is typically formed by collisions between accelerated electrons with the entering gas molecules, such as Ar, O_2, Cl_2, BCl_3, CF_4, CHF_3, SF_6, etc. These collisions lead to formation of ions and free radicals via ionization and dissociation processes, respectively. For example, electron collision with a tetrafluoromethane (CF_4) molecule can result in the following reaction:

$$CF_4 + e^- \rightarrow CF_3{}^+ + F + 2e^-.$$

This is only one example of the many other reactions occurring to CF_4. Therefore, in a RIE process, one has to consider a variety of ion groups, including $CF_x{}^+$, $C_2F_x{}^+$, F^+, as well as their negatively charged counterparts. Both positive and negative ions can participate in the etching processes, since the substrate is placed on a RF-biased electrode, which helps avoid charging of the sample.

The two main mechanisms to generate plasma are based on accelerating electrons with a parallel plate capacitor (capacitive coupled plasma or CCP) and with an induction coil (inductive coupled plasma or ICP). Historically, ICP RIE was invented later and hence this approach is more advanced than CCP. The development of ICP was mainly fueled by the industrial needs to achieve high-throughput etcher. ICP systems can generate plasma with extremely high densities, up to 10^{12} ions/cm^3, which is several orders of magnitude larger than the plasma densities in a CCP system. ICP RIE architecture was also designed to have

a plasma source, ICP torch, outside of the main reactor. Hence, ICP machine design provides a separate control over ion energy and ion density.

Developing an etching recipe from scratch is a challenging task, however, here we would like to offer general strategies for achieving HAR structures with low sidewall roughness. HAR structures require a more anisotropic etch, which can be achieved by increasing ion kinetic energy and reducing their scattering by gas molecules. Therefore, increasing bias voltage and reducing gas pressure (~10 mTorr) generally lead to more vertical and smoother etch profiles. Additionally, sidewall passivation can be instrumental in further straightening of the walls by impeding lateral etching. The sidewall passivation is implemented by adsorption of carbon- and/or oxygen-containing molecules, which emanate either from photoresist mask erosion or as a constituent of the feeding gases. Passivation comes with the price of sidewall contamination, although there are existing approaches to remove the passivation layer, for instance, with a hydrogen plasma treatment [131]. Since Cl does not attack SiO_2, the oxide sidewall passivation layers may also form due to Si contaminants in the etching chamber during RIE based on Cl chemistries [70,132]. For the etching chemistries with Cl or F compounds, isotropic etching can also be suppressed by substrate backside cooling [133].

Numerous studies have demonstrated that conventional ICP RIE techniques can be used to fabricate HAR subwavelength optical structures from various materials with an AR up to 15 [62,122,126,134]. Here, we take RIE fabrication of broadband dielectric metalenses as an example [122]. The fabrication protocol mainly includes deposition of amorphous silicon film on top of quartz substrates; patterning of Al_2O_3 mask on top of the film; and dry etching through the mask followed by mask removal (Figure 11.11(a)). The etching process was performed inside an ICP RIE chamber with feed gases of SF_6 (40 standard cubic centimeters per minute or sccm) and O_2 (16 sccm). This is a standard chemistry used for etching deep trenches in Si, where sulfur fluoride ions act as etching reagents. Al_2O_3 is known to be extremely resistant to SF_6-based etching, and its selectivity to Si reaches 1:70,000 [135]. In addition, during the etching process, the substrate was kept at –100°C to retard the fluoride isotropic etching reaction. The fabricated

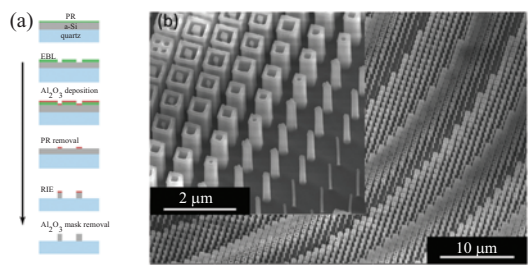

Figure 11.11 (a) Fabrication sequence for constructing Si-based metasurface. (b) SEM image depicting meta-atoms comprising broadband achromatic metalens, AR ~ 14, smallest feature size 100 nm [122].

metasurface is composed of 1.4-μm-tall meta-atoms having various shapes (Figure 11.11(b)). The smallest feature size is about 100 nm and it manifests a maximum AR of approximately 14. To the best of our knowledge, this is the largest AR value realized in metasurfaces.

Due to its wide availability, RIE is an attractive technique for implementing HAR nanophotonic structures. It is a relatively simple fabrication procedure typically consisting of only a few steps including mask patterning, etching, and mask removal. RIE is also a fast process with typical etching rates of about 100 nm/min. On the other hand, development and optimization of dry etching recipes, in particular for nonstandard materials, can be a time-consuming process. Often, the process is also sensitive to chamber contamination, which can be a major hurdle to maintaining process reproducibility especially in university foundries. Additionally, RIE is not suitable for etching metals such as Ag, Fe, Au, Ni, Co, and Pt, as their halides are nonvolatile compounds. The other common issue with RIE is the dependence of etching rate on feature size and pattern density due to the microloading effect. For instance, larger size openings and isolated standing structures etch faster than smaller and densely packed features.

RIE anisotropy can be further enhanced by increasing mask thickness. For instance, a thick hard mask can filter out most of the ions with a lateral momentum component. The inset of Figure 11.12(a) depicts two ions, where the first ion, incident at an angle, gets stuck by initially hitting the mask walls whereas the second ion, moving vertically, penetrates through the mask and impinges on the film surface. High *et al*. proposed and utilized this approach to etch epitaxially grown silver films and fabricated hyperbolic metasurfaces [136]. This visible-frequency metasurface was realized as a subwavelength grating with a width and height of 90 and 80 nm (AR ~ 1), respectively (Figure 11.12(b)). As previously mentioned, it is difficult to chemically etch metals since their halides (etching reaction products) are typically nonvolatile components. Thus, physical ion bombardment, for example, with Ar^+ ions is a viable solution to patterning silver. Physical etching with inert gases eliminates structure contamination. However, the etching process lacks selectivity and, therefore, thick masks made of hard materials, like aluminum oxide, are required.

11.3.1.2 Conformal atomic layer deposition on a template

As an alternative to the traditional approach of etching through a mask, HAR structures can be formed by conformally filling mask openings with the material of interest. For instance, conformal filling can be achieved by ALD, a vapor-phase technique capable of coating the substrate surface with layers whose thickness is of atomic precision. In 2016, Devlin *et al*. used the ALD-assisted patterning approach to produce dielectric metalenses in the visible spectrum [6]. Figure 11.13(a) illustrates the process flow, which includes the steps of patterning photoresist with EBL, ALD filling of titanium dioxide, and removing the capping layer with RIE.

More specifically, electron beam resist was spun onto a fused silica substrate, where the resist thickness defined the height of the final nanostructures. Afterwards, the resist was patterned with EBL to form a template. During the ALD

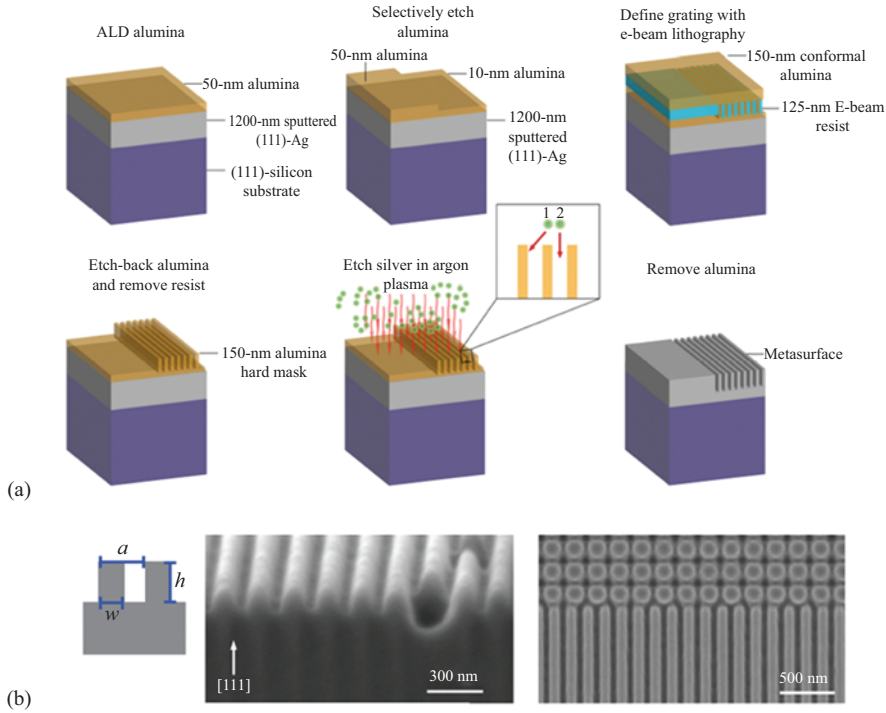

Figure 11.12 *(a) Process cycle for transferring HAR anisotropic patterns into a metal film. (b) SEM images of fabricated hyperbolic metasurface [136].*

process, the template was covered conformally with a layer of TiO_2. The ALD was terminated when the TiO_2 layer reached a thickness equal to half of the nanofin width. In a more general scenario, the ALD layer should be thicker than half of the maximum mask-opening width to ensure complete template filling. In the end, RIE was utilized to remove the residual TiO_2 capping film formed on top of the template surface and the resist was later dissolved to release the final metasurface.

The fabricated nanofins are 40 nm wide and 600 nm tall with an AR of 15, an almost impeccable sidewall angle of 89°, and miniscule RMS roughness of less than 1 nm (Figure 11.13(b) and (c)). Such smooth nanostructures were achieved due to the accurate monolayer-scale deposition control inherent to the ALD procedure, as well as that TiO_2 forms an amorphous-phase free-of-grain boundaries. Overall, this ALD template-filling technique can deliver spectacular fabrication results. However, on the downside, ALD is a slow process (~0.5 nm per cycle) and therefore cannot be used to generate large structures.

The ALD technique can also be applied to the construction of ultra-small gaps in metallic structures, which can produce significant electromagnetic field enhancement [137]. The process flow is illustrated in Figure 11.14(a). The first

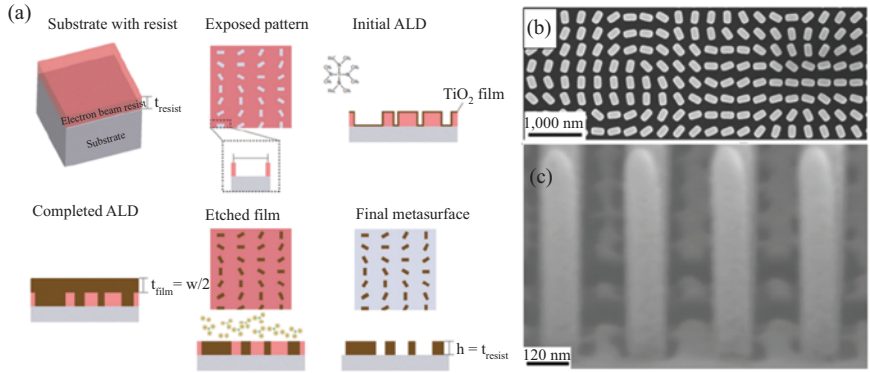

Figure 11.13 Fabrication of dielectric metasurfaces by conformally filling the resist-defined template with titanium oxide. (a) Process flow including the steps of EBL, ALD filling resist openings with TiO_2, and RIE of the extra material on top. (b) Top and (c) side views of the implemented metalens segment containing nanofins with various rotation angles. Nanofins are 600-nm tall with the smallest feature size of 40 nm (AR of 15) and smallest gap of 6 nm [6].

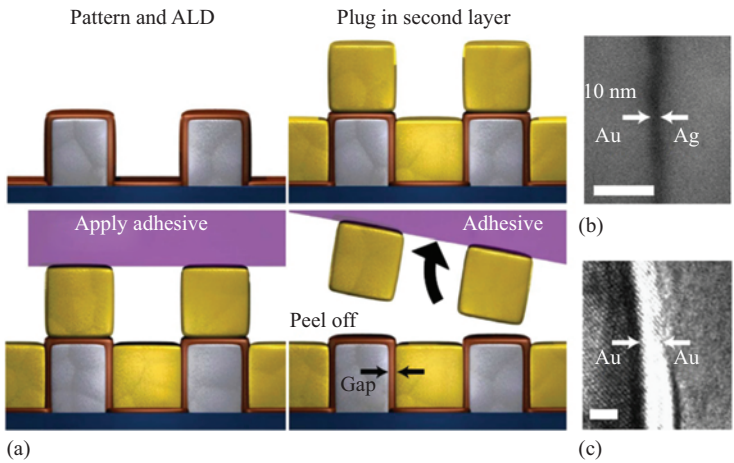

Figure 11.14 (a) Fabrication steps for constructing ultra-narrow plasmonic gaps. The procedure consists of two metal depositions, ALD conformal coating, and applying an adhesive tape to remove residual material. Cross-sectional SEM and TEM images of a (b) 10-nm and (c) 1-nm Al_2O_3 barrier inside the metal film [137].

metallic layer (colored in silver) was patterned by EBL, for example, into rectangular trenches. ALD was then utilized to conformally cover the whole pattern with a layer of dielectric (Al_2O_3), which in principle can be atomically thin. The gap size of the final structure is dictated by the ALD-layer thickness. Afterwards, the secondary metallic layer (shown with gold color) was directionally deposited. An adhesive tape was then attached on top of the structure. Since the tape only contacts the upper metallic layer, peeling off the tape selectively removes the upper layer and planarizes the whole structure. The resulting surface can be further smoothed by chemical-mechanical polishing.

As a result, a metallic film with ultra-narrow gaps of arbitrary forms and thicknesses can be constructed. Figure 11.14(b) and (c) displays SEM and TEM images of the fabricated 10 and 1 nm gaps. It is worth mentioning that the 1 nm gap was engraved in a 150-nm-thick planarized Au film, and thus the structure boasts a record large AR of ~150. The ALD coating further guarantees uniformity of the nanogaps, even when the first metallic layer comes with residual roughness after the patterning step. Additionally, this method enables the definition of gaps sandwiched between dissimilar materials, for instance, Au and Ag (Figure 11.14(c)). On the flip side, the sidewalls of the patterned metallic film must be vertical in order to physically separate the upper layer patterns and the structures located inside the initial openings. This condition is necessary for the peeling off step to work properly.

11.3.1.3 Metal-assisted chemical etching

Wet etching processes can also be employed to fabricate deep anisotropic patterns. One of such methods for achieving extremely HAR structures is metal-assisted chemical etching (MACE). In this technique, etching anisotropy originates from the metal-induced oxidation of a semiconductor material underneath and subsequent etching of the formed oxide. Typically, in MACE process, Au and Ag serve as catalyzers, H_2O_2 acts as an oxidant, and HF is an acidic solution to etch the oxide [138,139]. The typical MACE flow is depicted in Figure 11.15(a). Au is first patterned on top of a Si substrate. The etching process underneath the pattern produces vertical or porous pillars depending on consumption of generated holes at the Au-Si

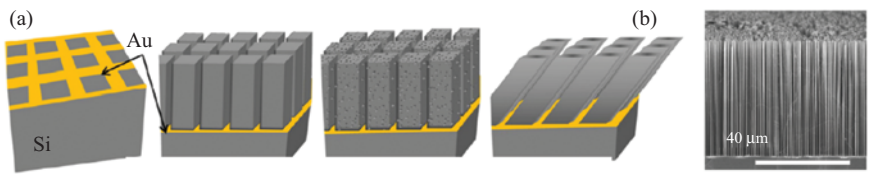

Figure 11.15 *(a) Illustration of MACE technique principle, from left to right: metal pattern on top of the semiconductor; possible outcomes: vertical, porous, and slanted pillars [141]. (b) SEM image of 550-nm diameter Si nanowires with height of 51 µm, showing AR of ~93 [140].*

interface. Additionally, at certain HF/H_2O_2 ratios the etching can lead to the formation of slanted pillars due to anisotropic etching rates along different crystallographic planes of Si. Figure 11.15(b) [140] shows an SEM image of the fabricated Si pillar array with an AR of 93.

In several studies, it was observed that vertical etching rate can be increased by reducing pattern period while horizontal etching rate and sidewall roughness depend on HF/H_2O_2 concentration ratio. High concentration H_2O_2 generates an excess of holes that cannot be consumed by HF, which increases roughness, while low concentrations of H_2O_2 limit the etching rate. Additionally, a low temperature environment can reduce roughness on sidewalls at the expense of much lower etching rates [142]. Typically, MACE minimally attaches the structure sidewalls and thus it can produce nanostructures with low-surface roughnesses of ~1 nm. Compared with other wet etching methods, the strongly anisotropic characteristic of MACE underpins its ability to achieve HAR. Nevertheless, MACE can only be applied to a narrow range of semiconductor materials, such as Si, Ge, GaAs, GaN, and InP, which limits its applications. Its etching direction depends on the material crystallinity and therefore only produces random structures when applied to etching polycrystalline materials.

Several variants of the standard MACE process were devised to overcome the drawbacks. For example, vertical directionality controlled MACE (V-MACE) [143] uses additional electron-hole-concentration balancing structures located in regions with large electron-hole concentration differences to restrict movement of metal catalysts, resulting in uniform etching rates and HAR structures. Inverse MACE (I-MACE) [144] uses a thick and insoluble oxide layer formed at the metal/semiconductor interface to serve as a barrier and limit hole injection in the vertical direction. In this way, semiconductor regions not interfaced with the catalyst layer can be etched preferentially. The resulting HAR structures can be narrower than the metal patterns with smooth sidewalls independent of the metal pattern edge roughness. Self-anchored-catalyst MACE (SAC-MACE) [145], which uses a nanoporous catalyst film to produce nanowires through pinholes, can confine the etching direction and enhance etch rate by increasing liquid access paths. This method can also etch through poly-Si/oxide/poly-Si stacks. Magnetic field-guided MACE (h-MACE) [146] enables the formation of periodic arrays of holes using isolated metal catalysts. HAR structures produced using the approach show applications over a broad range. For example, Si microwire with 2 μm diameter and an AR of 11.6:1 was fabricated by reducing the diffusion distance [147]. Divan *et al*. introduced a Ti adhesion layer to stabilize the migration of Au structures, a process used to fabricate linear Fresnel zone plates [148]. We foresee that further improvements of the versatile MACE process will facilitate its application in a broad range of areas.

11.3.2 3D structures

Conventional photonic devices are structured from thin films on flat substrates and are therefore 2D in nature. 3D structures make use of the underutilized third

dimension and can offer unprecedented degrees of freedom for optical designers. Apparently, 3D structure fabrication demands novel fabrication schemes. Such 3D fabrication can, in some cases, leverage planar fabrication methods, while in some other scenarios unconventional routes are pursued. In this section, we sample a few examples of 3D fabrication technologies relevant to subwavelength optics processing.

11.3.2.1 Two-photon polymerization

Two-photon polymerization (TPP) takes advantage of highly localized nonlinear absorption in optical polymers to achieve high-resolution layer-by-layer object construction and serves as a versatile platform for fabricating 3D micro- and nanostructures [149]. In this approach, an ultrashort laser is focused into a photosensitive monomer and scanned along a design profile to cure the material. Nanophotonic fabrication poses stringent requirements on the TPP process in terms of resolution, dimensional accuracy, geometry fidelity, surface roughness, and position accuracy. In order to improve the fabrication quality, optimization with main control parameters of the TPP process (i.e., numerical aperture of the objective lens, laser power, and exposure time) have been performed to enhance resolution [150–153]. Geometry deformation is addressed by pre-compensating for structure shrinkage [154] and utilizing multi-path scanning and 2D slicing methods [155], [156]. Additionally, surface roughness can be improved by increasing overlapping between adjacent voxels [157], dividing a 3D microstructure into several sub-regions with different slicing thicknesses [158], and angular and equal-arc scanning methods [159,160]. The main limitations of TPP are associated with the relatively low-refractive indices of polymer materials as well as manufacturing throughput and scalability.

Such a maskless lithographic approach allows free shaping of complex 3D structures with high resolution (below 100 nm) for precise definition of subwavelength devices [153]. An array of photonic applications have been enabled with additional degrees of freedoms not available from conventional microfabrication methods, such as micro-optics [161–165], diffractive optics [166], 3D photonic crystals [166–168], light cages [169], phase masks [170], AFM probes [171], etc. Functional optical systems typically require more than one optical component while conventional assembly techniques developed for discrete optical components cannot provide sufficient precision and cost effectiveness for integration of subwavelength optics. TPP can potentially address this issue by monolithic fabrication of multiple elements without additional assembly steps. As demonstrated in [163] (Figure 11.16(a)), objectives consisting of stacked micro-lenses were developed, in which the multiple stages of aspheric lenses were written along with mechanical supporting structures using TPP, enabling monolithic integration of micro-scale high-performance optical systems immune from assembly misalignment.

3D photonic crystal structures with a total of 40 layers have been fabricated using TPP [167] (Figure 11.16(b)–(d)). Again, mechanical considerations were incorporated in the structure design to minimize distortions due to polymer

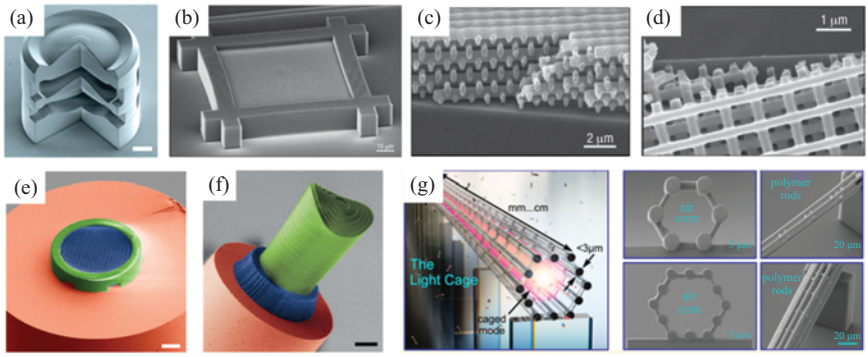

Figure 11.16 Implementation of TPP in micro- and nano-photonic device fabrication: (a) nano-printed triplet lens system (scale bar, 20 μm) [163]; (b)–(d) 3D photonic crystals with a total of 40 layers and surrounding walls written to prevent bending and reduce distortions due to polymer shrinkage during polymerization [167]; (e) a chiral photonic crystal structure for polarization control directly on an optical fiber tip (scale bar, 10 μm) [166]; (f) a free-form lens with patterned Fresnel zone plate for beam shaping on a fiber (scale bar, 25 μm) [166]; (g) schematic and fabricated light cage structures [169].

shrinkage during polymerization. In [166], chiral photonic crystals with an inter-layer distance of 400 nm were fabricated directly on an optical fiber tip for polarization control (Figure 11.16(e)). A free-form lens structure with Fresnel zone plate was subsequently fabricated on top of the photonic crystal structures for beam shaping (Figure 11.16(f)). This multi-scale photonic system is an excellent example showing the fabrication and integration versatility offered by TPP. Hollow core light cages fabricated by TPP were demonstrated [169], which consist of 6 or 12 free-standing polymer strands of 3 μm diameter around a central hollow core (Figure 11.16(g)). The light cage was written over 1 cm distance with diffraction-less propagation in the UV, visible, and near-infrared spectral regimes and high confinement of the fundamental mode. Such a platform is attractive to spectroscopic sensing and bioanalytics when integrated with optofluidic devices.

11.3.2.2 Interference lithography

Interference lithography (IL) (also known as holographic lithography) exploits the interference of two or more coherent laser beams to pattern fine features (below 50 nm) over large areas [172–177], which is of particular interest to large-scale fabrication of nanophotonic devices. Assuming a laser wavelength of λ and a refractive index of n for the immersion material, the minimum achievable feature size with a single exposure has a half-pitch of $\lambda/4n$.

The basic method of generating interference patterns for subwavelength optics fabrication involves multiple exposures [172,178] or multiple beams [179]. 3D

photonic crystals have been realized using holographic lithography based on multibeam interference in a photoresist. Large-area, sub-micron structures were demonstrated [176,180]. With four non-coplanar beams from holographic lithography, diamond-like structures were fabricated with beams from all spaces [181]. Using five beams, the diamond-like structure can be created with only beams from half spaces [182,183].

In addition to bulk optical components, interference patterns can also be generated by passing the laser beam through a diffraction element mask [175,184–190]. For instance, multi-layer phase masks with orthogonally oriented gratings produced in a liquid crystal and photoresist mixture were developed to generate five-beam interference patterns [191] (Figure 11.17(a) and (b)). Diamond-like photonic crystal structures were created by exposing photoresist mixtures to the interference patterns formed by the phase mask (Figure 11.17(c) and (d)). Phase-engineered interference lithography can also be achieved using programmable spatial light modulators [192–198].

11.3.2.3 Membrane projection lithography

Membrane projection lithography (MPL) is an emerging method for fabrication of metamaterials and metasurfaces consisting of 3D unit cells [199–203]. As

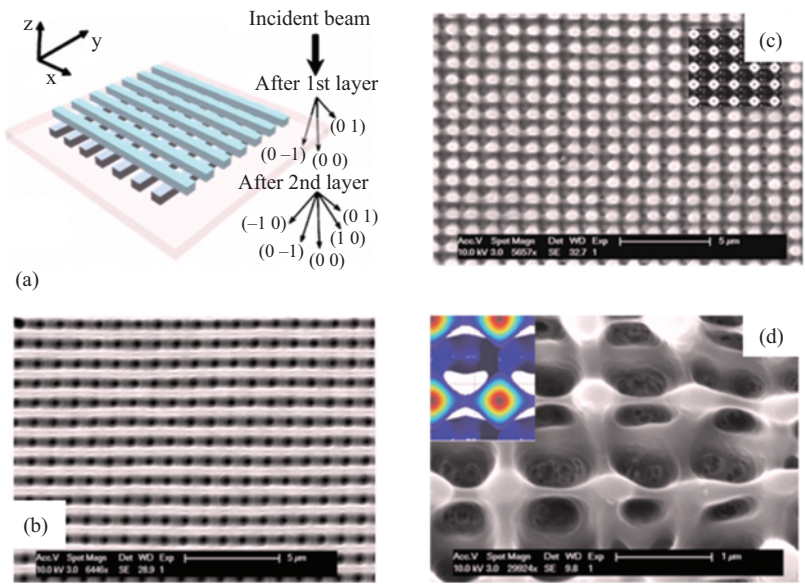

Figure 11.17 *(a) Schematic of multi-layer phase mask IL setup [191]. (b) SEM of fabricated multiple-layer phase mask. (c) SEM of fabricated 3D photonic crystal structure using multi-layer phase mask IL method. (d) Enlarged view of the photonic crystal structure. Inset is the simulated five-beam interference pattern [191].*

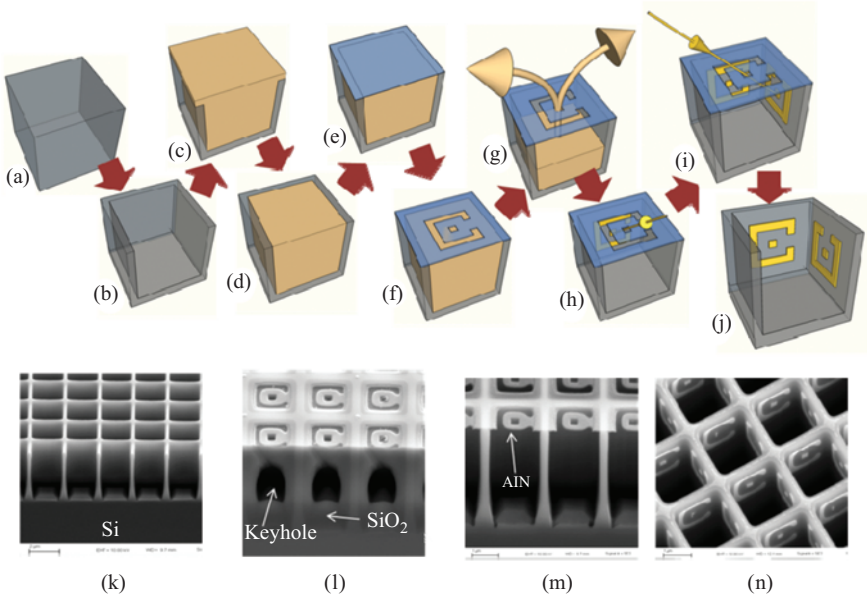

Figure 11.18 *(a)–(j) Fabrication process flow of membrane projection lithography. (k) SEM image of cubic silicon cavities; (l) SEM image of backfilled cavities and patterned membrane; (m) SEM image of unit cells with patterned membrane suspended over cavity; (n) SEM image of final unit cells decorated with gold SRRs on sidewalls [199].*

schematically illustrated in Figure 11.18 [199], a unit cell cavity was first etched into a Si substrate and backfilled with a sacrificial material. After the top surface was planarized using chemical-mechanical polishing (CMP), a membrane layer is deposited and patterned with through holes of target geometries. After the sacrificial layer is removed through wet etching, the membrane becomes a suspended shadow mask layer. Directional material depositions such as metal evaporation are then conducted to "decorate" the unit cell by projecting the membrane patterns onto the unit cell sidewalls. The "decoration" step can be repeated with different deposition flux directions to create patterns on multiple sidewalls. The membrane is finally removed to complete the fabrication process.

The CMOS compatible MPL process can be applied to generate a suite of unit cell geometries and sidewall pattern shapes such as vertically oriented split ring resonators (SRR), in metallic or dielectric materials. Structures with a linewidth down to ~100 nm have been demonstrated using MPL. The technique can also be adapted to fabricate 3D stacked photonic structures through layer-by-layer processing.

11.3.2.4 DNA-assisted nanoparticle assembly

Deoxyribonucleic acids (DNAs) are widely known as the essential components of all living creatures. These macromolecules serve as long-term storage of genetic information necessary for organism functioning, development, and reproduction. Back in 1996, it was proposed that DNAs can also be employed in programmable materials synthesis [204–206]. More specifically, rigid inorganic nanoparticles (NP) functionalized with DNAs can rationally conjugate to form self-organized structures ranging from microscopic molecule-like assemblies to macroscopic crystallographic arrangements [207,208]. Principle of binding gold colloids via DNAs is illustrated in Figure 11.19(a). The process typically consists of two steps. During the first phase, anchor-DNAs are attached to NP surface (illustrated as fully

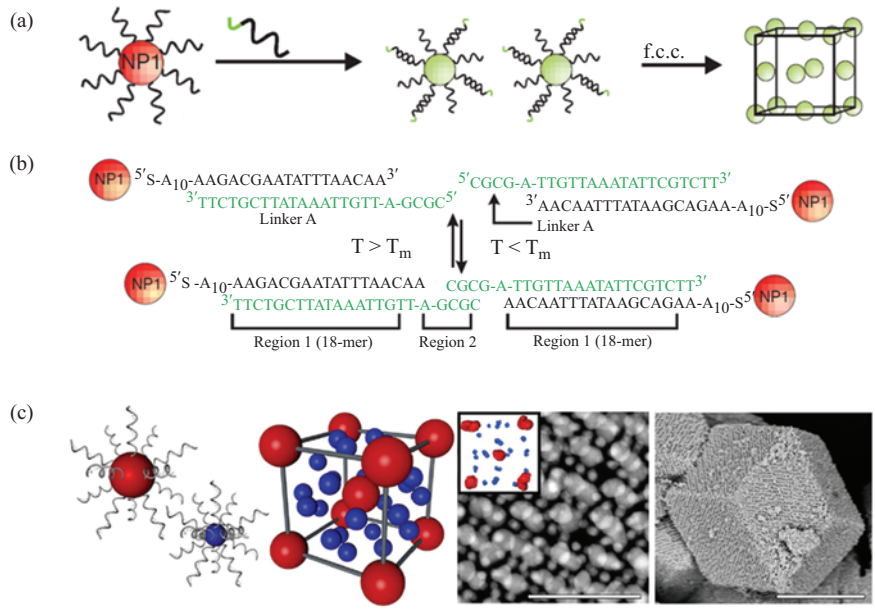

Figure 11.19 *(a) Gold colloids functionalized with DNA chains can be controllably connected with each other to form molecule- and crystal-like structures. (b) Detailed depiction of DNA binding procedure to form a binary NP molecule. Two molecules, each consisting of 18 nucleobases (black font color), directly anchor to the NPs. Then two linkers, each composed of 23 nucleobases (green font color), attach to the latter DNA strands (region 1) and connect with each other (region 2) via DNA base-pairing rules [207]. (c) Schematic of binary-component NP superlattice, TEM image of the Cs_6C_{60} isostructural lattice and SEM images of fabricated CsCl-lattice microcrystals, respective scale bars are 50 nm and 1 μm [208,209].*

black strands sticking out from an NP). In the second step, linker-DNAs are introduced (indicated as black strands with a green subsequences) in order to form a complete binding between the NPs. Figure 11.19(b) provides a detailed example of such a binding where four nucleotide sequences intertwine with each other and form three paired regions. Interestingly that DNA crosslinks can be reversibly disassembled if the substance is heated above the link (region 2) dissociation temperature [204]. The DNA-based conjugation approach can be extended further to bind together particles of different sizes to form various superlattices. Examples of the NP crystallographic arrangements mimicking lattices of Cs_6C_{60} and CsCl are demonstrated in Figure 11.19(c) [208,209]. DNA-assisted self-assembly is a very attractive technique due to the highly advanced capabilities of DNA synthesis, which allows automated generation of DNAs chains of arbitrary lengths and surface binding functionalities [210].

11.3.3 Fabrication on unconventional substrates

To date, most subwavelength optical structures are fabricated on flat, rigid substrates exemplified by silicon wafers. There is, however, growing interest in deploying these devices on unconventional, non-planar substrate platforms for many emerging applications. For example, integration of metasurface optics on arbitrary free-form substrates can decouple the optical capabilities of the component from its geometric configurations, the latter of which being dictated in many cases by considerations other than optical functions (e.g., hydrodynamics) [13,211–213]. For example, flexible devices built on mechanically compliant substrates with elastic properties matching those of biological tissues potentially enable minimally invasive biomedical sensors and actuators suitable, for instance, for conformal integration on human skin [214–217]; stretchable photonic and plasmonic structures provide a facile way for strain-mediated optical tuning and reconfiguration [218–223]; and nanostructures on the end facet of optical fibers can impart functions including antireflection, beam steering and shaping, optical coupling and sensing [224].

These tantalizing new capabilities nevertheless come with the price of added processing complexity. Tailoring standard optical and electron beam lithographic tools to patterning on these unconventional substrates is an applicable path in some cases, although the benefit is apparent only when extensive process customization is not mandated. Alternatively, the subwavelength structures can be fabricated on a flat handler substrate using classical methods and then transferred onto the unconventional substrates. Maintaining pattern fidelity, yield, and throughput constitutes the key to implementing a successful transfer process. Another popular alternative is to use direct laser beam or ion beam writing methods, although throughput and accuracy represent inherent trade-offs for these beam-based techniques. Simply put, there is no "universal" solution that applies to all substrate platforms, and in the following we will review the technology choices for different substrate classes.

11.3.3.1 Integration on flexible and stretchable substrates

Flexible and stretchable substrates are usually made of organic polymers and elastomers. Manufacturing electronic devices on these substrates has matured over the past several decades and is now a fairly well-established process [225]. However, printing or standard photolithography is routinely used for metal interconnect fabrication. When it comes to inorganic semiconductors, transfer printing becomes the preferred integration route [226,227].

These techniques can be adapted to subwavelength optics fabrication although process modifications are often mandated given the unique characteristics of optical devices [66,228–231]. For instance, unlike most electronic devices, optical devices are extremely sensitive to misalignment between the structural units, which readily modifies optical coupling. The sensitivity is further amplified in subwavelength optics due to strong field concentration common in these structures such that even displacements of a few nanometers can drastically change the device response. While the phenomenon has been harnessed for efficient optical tuning [232,233], it poses stringent requirements on pattern fidelity in particular to transfer printing methods, which are more prone to misalignment.

The technical challenge associated with misalignment can be obviated using anchored or interconnected subwavelength structures. As an example, Zhu *et al*. fabricated flexible high-contrast gratings (HCGs) exhibiting strain-tunable colors using the transfer printing method (Figure 11.20) [234]. The HCGs were patterned from an SOI wafer using SiO_2 as a etch mask. The structures were then released from the substrate through an HF vapor etching step, picked up from the substrate using a flat PDMS slab, and capped using a second PDMS layer. To ensure a high transfer yield, the HCGs assume the form of 100 μm × 100 μm pixel arrays, and the pixels are connected to a supporting frame with folded beams to minimize pattern distortion during structural release. The folded beams readily rupture during the PDMS delamination step without affecting the HCGs structures. Similarly, partially etched pedestals can be used to tether isolated structures (e.g., individual waveguides, meta-atoms, or nanoantennas) prior to their complete release from the handler substrate, thereby preventing undesired displacement or deformation

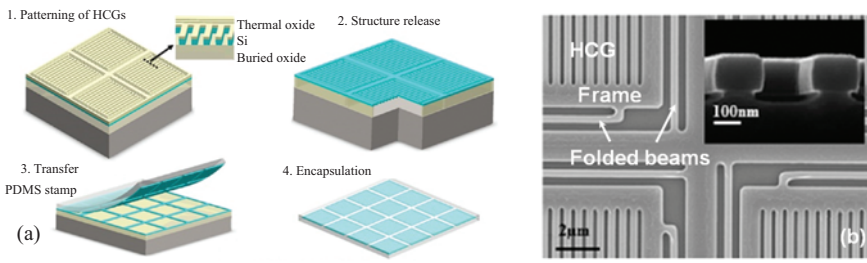

Figure 11.20 (a) Transfer printing of high-contrast gratings onto flexible substrates; (b) SEM image of the HCGs on SOI substrate after etching: inset shows the HCG cross section [234].

during transfer [235]. It has been demonstrated that the transfer printing process can be applied to create large-area (10 cm × 10 cm) structures on virtually arbitrary substrates [236].

Another commonly adopted method for subwavelength optics fabrication on flexible substrates involves first patterning the optical structure on top of a sacrificial layer on a rigid handler substrate, followed by encapsulation of the structure in PDMS elastomer, and finally delamination from the handler after removing the sacrificial layer [212,221,237]. Differing from the transfer printing approach, here PDMS is cast on the patterned structure and cured to encapsulate the entire structure. Figure 11.21(a) illustrates one instance of the process [212]. Here, a metasurface made of amorphous silicon (a-Si) nanopillars was first patterned using EBL and subsequent dry etching with an Al_2O_3 hard mask (Figure 11.21(b)). A two-layer PDMS film was then coated in two spin steps, the first with a diluted solution to enhance infiltration between the a-Si structures and the second with regular PDMS monomer. Once the PDMS layers were cured, the nanopillars were released from the handler wafer by wet etching of the Ge layer to form a free-standing, flexible metasurface structure. It should be noted that curing can lead to volume shrinkage of PDMS, and the resulting spacing change needs to be compensated for precise pattern pitch control [238].

An alternative to the transfer approach is direct patterning on flexible substrates. Metallic nanoantenna arrays can be readily deposited onto polymeric substrates via evaporation or sputtering and subsequent patterning using photolithography or EBL coupled with etching or liftoff [239–242]. The deposition process can also be masked to generate target patterns in a single step. For the masking purpose, nanosphere lithography [243–246] and block copolymer self-assembly [247] afford fine resolutions commensurate with subwavelength optical structure processing, although they only present limited options of possible unit cell shapes and lattice configurations. On the other hand, fine features of varying geometries can be formed using nanostencil lithography, an advanced shadow-masking

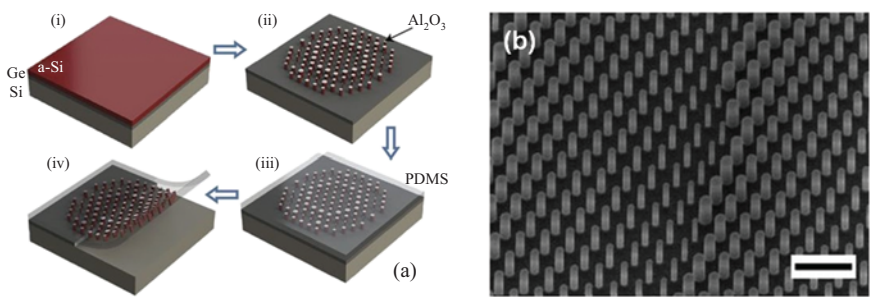

Figure 11.21 (a) Schematic fabrication process of a conformal dielectric metasurface; (b) an SEM image of the a-Si nanopillars with the Al_2O_3 mask before PDMS encapsulation; the scale bar corresponds to 1 μm [212].

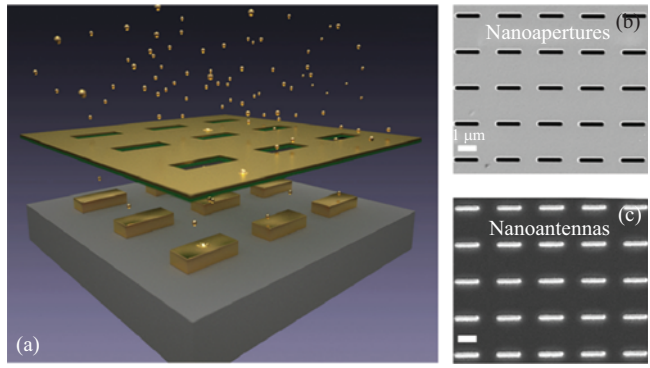

Figure 11.22 (a) Schematic illustration of the nanostencil lithography process; (b, c) SEM images of (b) the nanostencil and (c) fabricated nanoantennas [250].

technique (Figure 11.22) [248,249]. Plasmonic nanoantennas with a minimal feature size down to 25 nm have been experimentally realized using this method [248].

It is also possible to use a pre-patterned flexible substrate to template the subwavelength structures. Hokari *et al*. recently demonstrated embedded printing for sub-micron metallic structure fabrication [251]. The concept is depicted in Figure 11.23(a) [252]. The process began with imprinting a PMMA plastic substrate to form a groove pattern. The grooves were then filled with conductive ink containing metal nanoparticles assisted by capillary force. Once the residual ink outside the grooves was removed, the ink was sintered, transforming into solid metallic structures embedded in the plastic substrate (Figure 11.23(b)). It is worth noting that sintering results in dimensional changes of the metallic structures (Figure 11.23(d)), which must be properly taken into account to achieve desired optical functions (Figure 11.9(c)). Nanoimprint can be similarly combined with angled deposition to generate subwavelength plasmonic architectures [253].

Transfer-free fabrication of dielectric subwavelength structures on flexible substrates potentially offers the benefits of simplified processing as well as improved throughput and yield, albeit while imposing additional constraints on material selection. In addition to possessing high refractive indices and low optical loss, the dielectric material should also be amorphous or polycrystalline to facilitate epitaxy-free deposition on polymers. Moreover, the deposition process must be thermally and chemically compatible with the flexible substrate: oxygen-plasma-assisted sputtering of oxide thin films, for instance, causes damage to most polymers. Possible material candidates that meet the standards include a-Si and silicon nitride grown with special low-temperature processes [254–256], sol-gel oxides such as TiO_2 [257,258], and vacuum deposited [100,259–265] or solution derived chalcogenides [68,266–268]. Figure 11.24 illustrates an exemplary process flow for monolithic photonic device fabrication on polymer substrates. In this embodiment, the flexible substrate comprises a polymer film initially spin coated on a handler wafer, and the target patterns can be defined using standard lithographic methods,

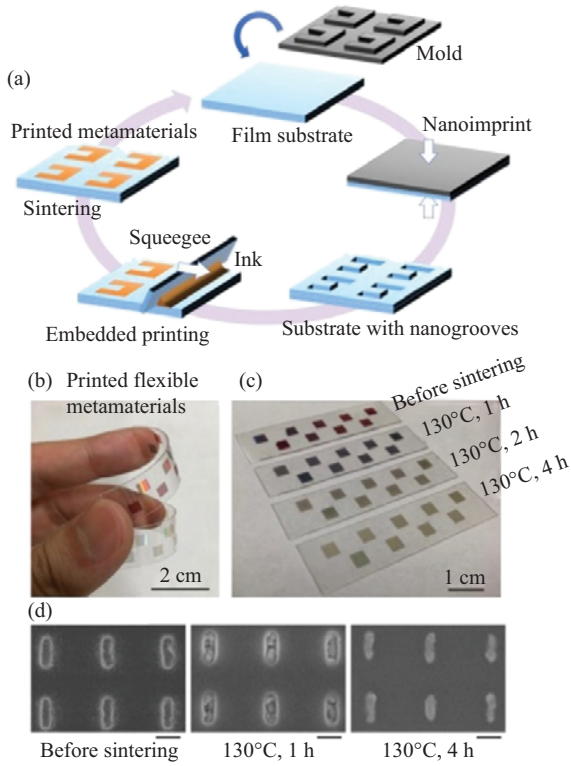

Figure 11.23 *(a) The embedded printing process; (b) printed flexible metamaterials; (c) photograph of printed flexible metamaterials before sintering and after sintering at 130°C for 1, 2, and 4 h; (d) SEM images of printed metamaterials for different sintering conditions. The black scale bars indicate 200-nm length [252].*

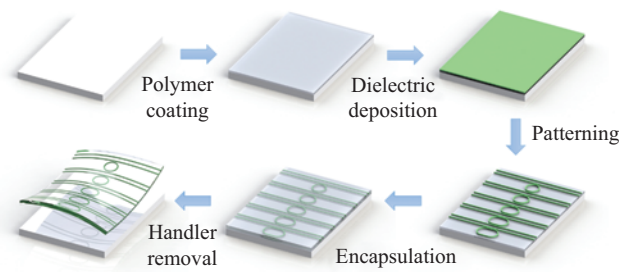

Figure 11.24 *A generic process flow for dielectric material deposition and device fabrication on polymer substrates [257].*

nanoimprint [269], or soft lithography. The optical structures are subsequently encapsulated and delaminated from the handler substrate to form a free-standing flexible device. A main advantage of the process is that it leverages standard nanofabrication infrastructures with minimal customization needed.

Additional challenges arise when it comes to dielectric material integration on elastomers. Elastomers typically exhibit gigantic coefficients of thermal expansion (CTE) that are one to two orders of magnitude larger than most dielectric and semiconductor materials. Take the most commonly used PDMS as an example; it has a tremendous linear CTE of 3.1×10^{-4}/°C [270], compared to those of Si (2.6×10^{-6}/°C), SiO_2 (0.55×10^{-6}/°C), and Si_3N_4 (3.2×10^{-6}/°C). To mitigate film delamination and cracking due to the large CTE mismatch, several measures can be taken. One option is to limit the thermal budget of the entire fabrication process, including that of the resist baking steps [271]. Other viable solutions include inserting a strain-releasing layer between the elastomer and the dielectric material [65,69,272] or arranging the dielectric structures into small isolated islands [273]. To accommodate the large elastic strain during stretching of elastomers, configurational designs matured in the stretchable electronics domain (e.g., serpentine line shapes and local substrate stiffening [274,275]) may be employed although optics-specific optimizations are often essential for photonic devices [69].

11.3.3.2 Subwavelength optics fabrication on non-planar and irregular substrates

Technologies for nanostructure fabrication on non-flat substrates can be generally classified into three categories: flexible membrane conformal integration, soft-lithography-based methods, and beam writing. In the first scheme, structures fabricated on a thin stretchable membrane are conformally attached onto a non-planar receiving substrate to impart the target functions, and the techniques described in Section 11.3.3.1 can be implemented for this purpose. In this section, we will therefore focus on the latter two approaches.

Soft lithography

Soft lithography is broadly defined as "a collection of techniques based on printing, molding and embossing with an elastomeric stamp" [276]. The elastomeric stamp can be readily deformed to conformally contact curved surfaces, enabling facile pattern transfer. A number of soft lithographic techniques have been applied to patterning on tightly curved surfaces with feature size down to 15 nm [277–282]. Figure 11.25(a) depicts the fabrication procedure of soft imprint molds capable of resolving such deep sub-micron features. The composite mold consists of three laminates: a PDMS/polyethylene terephthalate (PET) backplane and an epoxysiloxane imprint layer [283]. The soft PDMS/PET backplane can readily deform to conform to the shape of the substrate, whereas the epoxysiloxane film contains the replica molded features for imprint pattern transfer. Epoxysiloxane is a superior candidate for the imprint layer than the classically formulated PDMS given its larger stiffness, which minimizes pattern distortion during embossing. The mold

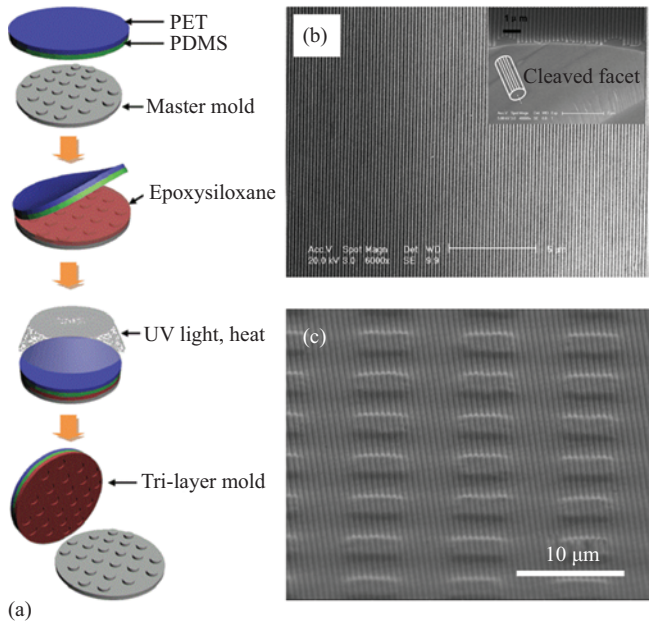

Figure 11.25 (a) Composite mold fabrication for imprint on non-flat surfaces [283]; (b) SEM image of 200-nm pitch gratings imprinted on the surface of a 125-μm diameter fiber; inset shows the cleaved facet of the patterned fiber [277]; (c) SEM image of imprinted 500-nm pitch gratings over a 500-nm-thick micro-post array [283].

can then be used to conformally imprint fine structures on curved (Figure 11.25(b)) or uneven surfaces (Figure 11.25(c)).

A variant of soft lithography (sometimes termed "optical soft lithography") entails creating an elastomeric photomask, through which a photoresist layer coated on a non-planar surface can be exposed to produce the target pattern [284–287]. So far, the minimum feature size of the method that has been experimentally validated is limited to 1 μm [284], which constrains the operation wavelength of viable optical structures. Notably, the method can also be utilized to generate gray-scale elastomeric masks [288].

Beam writing techniques

Focused energetic beams—laser, ion, or electron beams—can be used to either expose resist layers or directly inscribe patterns on non-planar or even irregular surfaces. For beam writing on a non-flat (or tilted flat) surface, the depth of field (DOF) that dictates the vertical distance over which the resolution of written patterns is not compromised is a critical parameter. For a focused laser beam, its field profile can be closely approximated with a Gaussian beam. Ideally, the focal spot (beam waist) should coincide with the substrate surface (or resist layer). Deviations

from ideal focusing results in diffraction and blurring of the written pattern. The DOF is given by the Rayleigh range z_R of the beam [289]:

$$z_R = \frac{\pi w_0^2}{\lambda} \sim \frac{\lambda}{\pi \cdot NA^2}, \tag{11.1}$$

where w_0 gives the beam waist size, λ is the wavelength, and NA denotes numerical aperture of the lens used to produce the focused beam. Equation (11.1) indicates a trade-off between resolution (w_0) and DOF: a tightly focused laser beam with large NA contributes to enhanced resolution at the expense of DOF. For typical laser writing experiments, the DOF is generally less than 1 μm. Given this small DOF, the laser must be dynamically refocused via precision motion stages to follow the surface morphology. Figure 11.26(a) schematically illustrates one embodiment of such a laser writing system customized for patterning on curved surfaces [290]. In addition to autofocusing, the system is also capable of dynamically adjusting the substrate tilt such that the laser beam is always perpendicular to the local substrate surface to minimize pattern distortion. Figure 11.26(b) and (c) shows images of diffractive optical elements fabricated on a lens surface using the equipment. The system's resolution, dictated by the focal spot size, is approximately 1 μm, although further resolution enhancement is possible with improved optics or use of two photon lithography. It is also possible to use quasi-non-diffracting beams such as

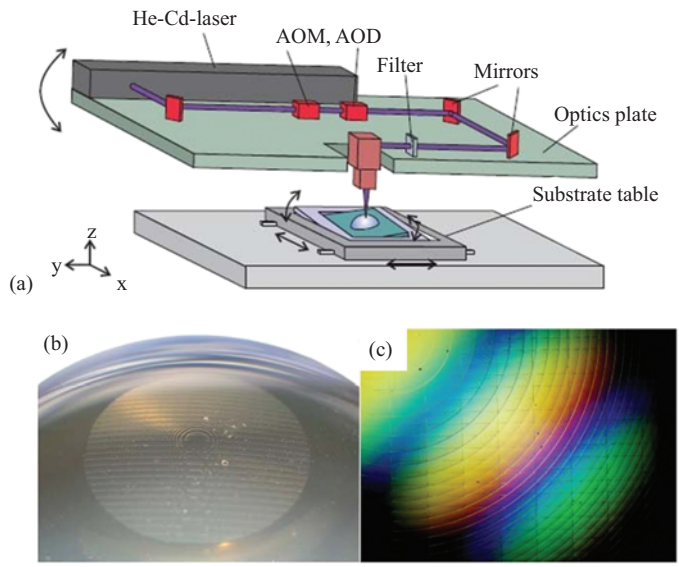

Figure 11.26 (a) A laser lithography system engineered for patterning on curved surfaces; (b) photograph of a diffractive element on a biconvex lens fabricated using the system; (c) microscope picture of the hybrid element taken in differential interference contrast mode [290].

Bessel beams or Airy beams to increase DOF with minimal loss in resolution [291], although their non-ideal beam profiles can be problematic for certain applications.

Electron beam and ion beam writing follow similar principles albeit with some important differences. Electron and ion beams have much smaller wavelengths than visible light: for electrons with 100 keV kinetic energy, their de Broglie wavelength is 0.039 Å, far smaller than that of lasers. These small wavelengths underlie the superior resolution of charged particle lithography. On the other hand, the NA of electron optics in EBL tools is small, typically on the order of 10^{-3}. The corresponding DOF calculated using the equation (11.1) is approximately a few microns. While the DOF is considerably larger than that of laser writing, the beam still needs to be refocused for samples with macroscopically non-flat features. Electron beam focus can be adjusted by dividing up the entire writing area into a number of smaller writing fields within which the height difference is smaller than the DOF [292], or constantly adjusted making use of the dynamic focusing function [293]. Compared to EBL, helium ion beam lithography has an even smaller NA, which contributes to its large DOF that can exceed 100 μm and facilitates patterning on uneven substrates [294].

Besides DOF considerations, one additional challenge for beam writing on non-flat substrates is how to obtain a uniform resist coating should a pattern transfer step be necessary. For a macroscopically curved substrate such as the surface of a lens with moderate NA, standard spin coating may work provided that the edge beads are properly taken care of. For irregular surfaces where spin coating fails, techniques including resist transfer [295], spray coating [296], evaporation [297,298], dry film resist application [299,300], plasma polymerization [301], the Langmuir–Blodgett method [302], and even the use of ice as a resist [303] have been implemented. As an example, Figure 11.27 shows structures written in thermally evaporated polystyrene resist on an AFM cantilever, highlighting versatility of the resist coating and patterning method [297].

Apart from focused particle beams, collimated ion beams can also be applied to patterning on non-planar surfaces. The technique is named ion beam proximity lithography (IBL). In IBL, a stencil mask is placed above the substrate and flooded with a collimated beam of energetic ions. Unlike focused beams, well-collimated ion beams offer an enormous DOF exceeding 1 cm [304,305]. Patterning of deep-submicron-sized features on non-planar substrates has been realized using IBL [306].

11.3.3.3 The tip of a fiber—a new dancing stage for photonic engineers

Having a size and form similar to that of an ordinary needle's point, the tip of a fiber is tiny from a macroscopic perspective. However, a fiber tip—a unique unconventional substrate with direct access to light—also presents big opportunities for photonic engineers. For instance, nanophotonic structures mounted on the fiber facet can reshape or redirect the output optical mode to modulate its spectral and/or spatial distributions, or facilitate coupling with other optical devices. Integration of photonic components on a fiber tip can also impart new

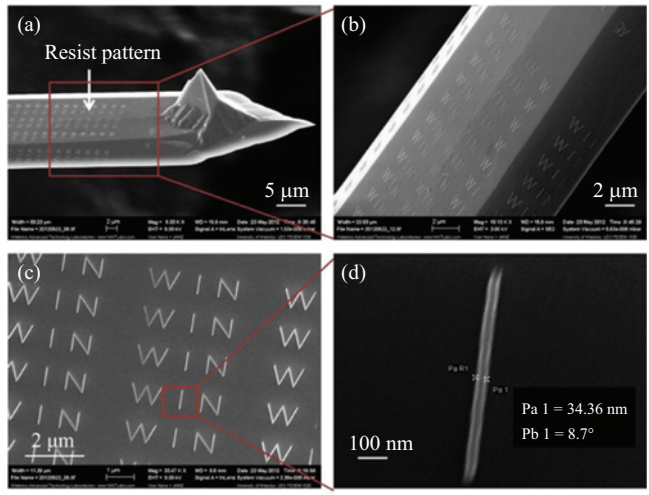

Figure 11.27 SEM images of patterned polystyrene resist on an atomic force microscope cantilever by EBL, taken at increasing magnifications from (a) to (d); the resist is deposited using thermal evaporation [297].

functionalities such as sensing and optomechanical manipulation, paving the path toward a versatile "lab-on-fiber" platform [307].

With its small cross-sectional area and a needle-like form factor, the fiber tip also presents unique challenges for subwavelength optical structure integration. It is possible to adapt most planar nanofabrication technologies for this purpose albeit with significant process customization. Alternatively, the structures can also be first fabricated on a standard planar substrate followed by transfer onto the fiber tip. Both approaches are elaborated further in this section.

Hybrid nanotransfer onto a fiber tip

By avoiding direct fabrication on a fiber tip, hybrid nanotransfer sidesteps the challenges linked to handling of fiber-associated widths during lithographic processing. In an exemplary process demonstrated by Smythe *et al*. [308], gold nanoantenna arrays were initially patterned on Si using EBL. The array was then stripped off the wafer using a thin polymer film, and attached onto a fiber facet along with the carrier film. In the last step, the sacrificial carrier is etched away, leaving the antenna array adhering to the fiber tip via van der Waals attraction. The fiber tip decorated with the nanoantenna array was used as an easy-to-use surface-enhanced Raman spectroscopy (SERS) probe operating in a reflective mode. In addition to SERS [309], metallic nanostructure arrays transferred onto fiber tips have also been applied to plasmonic refractive index sensing [310,311].

Other nanotransfer alternatives offer the added capability of aligning photonic structures to the fiber core. These methods are exemplified by the transfer of photonic crystal cavities onto fiber facets [312–315]. The processes in general involve release of a photonic crystal membrane from a handler substrate via sacrificial etching followed by transfer of the membrane via a micromanipulator [313,314] or direct gluing of the membrane to the fiber end [312]. Li *et al*. further extended the direct transfer approach by employing the transferred Si nanomembrane as a hard mask for subsequent patterning transfer [316]. Figure 11.28(a) depicts two variants of the process where the patterned Si membrane is first picked up from the starting substrate using a tungsten tip with PDMS adhesive, and then transferred to the final substrate to mask (i) etching or (ii) liftoff. Once the pattern transfer is complete, the mask is removed and can be reused multiple times. As a proof-of-concept, the authors implement the technique to pattern gold dot arrays aligned to a fiber core (Figure 11.28).

Here, we conclude this sub-section on nanotransfer by highlighting an impressive piece of work by Arce *et al*., where they transferred an entire SOI photonic circuit to realize a fiber-tip-integrated refractive index sensor [317]. As shown in Figure 11.29, the compact photonic circuit encompasses a focusing grating coupler optically interfacing with the fiber core, a multimode

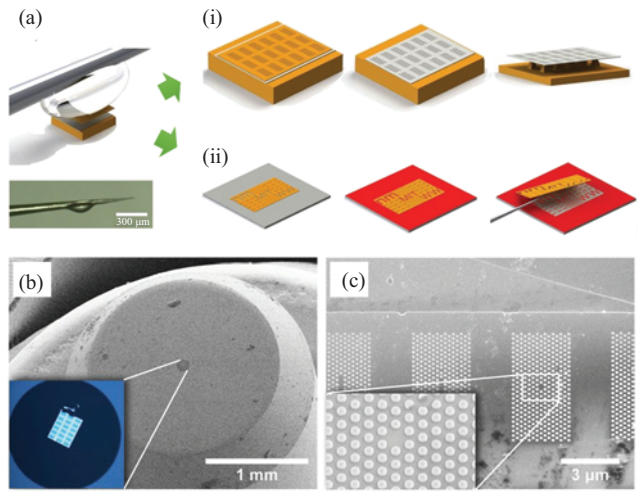

Figure 11.28 *(a) Hard mask transfer process for (i) etching and (ii) liftoff; inset shows the image of a tungsten tip with attached PDMS adhesive used to pick up and position the nanomembrane mask; (b) a silicon membrane with patterned gold dot arrays on a fiber facet; inset shows an expanded view of the membrane on the fiber core; (c) patterned gold dot arrays on the fiber facet after removal of the nanomembrane mask using a tungsten tip; inset gives an expanded view of the gold dots [316].*

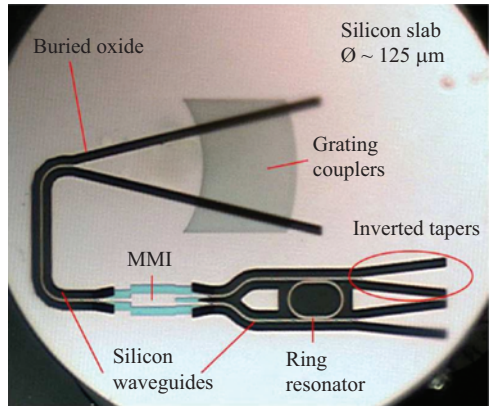

Figure 11.29 Top-view micrograph of a silicon photonic circuit integrated on a fiber tip [317].

interferometer, a racetrack resonator in an add-drop configuration, as well as inverted tapers to prevent back reflected light from coupling into the circuit. Both clockwise and counterclockwise propagating modes are excited by the bus waveguides such that the light is coupled back into the fiber to be analyzed. The demonstration reveals the possibility of integrating complex photonic functions onto the fiber tip to enable versatile fiber probe sensing systems.

Adapting planar nanofabrication techniques to direct patterning on a fiber tip

Over the past two decades, most standard wafer-scale manufacturing technologies have been adapted to photonic fabrication on a fiber tip. These methods include optical, electron beam, and ion beam lithography, nanoimprint, and laser direct writing. Unlike self-assembly based bottom-up methods [318–320] or photopolymerization using light guided in the fiber [321], top-down fabrication schemes are capable of reproducibly generating structures with well-defined geometry essential for many nanophotonic device applications.

For optical lithography and EBL patterning on a fiber tip, preparing a uniform resist coating on the fiber end sets the first technical challenge. Methods described in Section 11.3.3.3 for resist coating on irregular substrates such evaporation are equally applicable to fiber tips [322]. Resist can also be applied using classical spin coating while the fiber being supported on special holders or fiber ferrules [323–326]. Another technique involves dip and vibration coating, where the fiber end is first dipped into liquid resist and the excess resist is then removed by mechanical vibration [327]. Subsequent exposure of the resist is performed using standard UV lithography [328], interference lithography [329,330], digital micromirror device (DMD) projection [326], or EBL [323]. The structured resist layer can either act as the optical element itself or serve as a mask for etch pattern transfer into the fiber material.

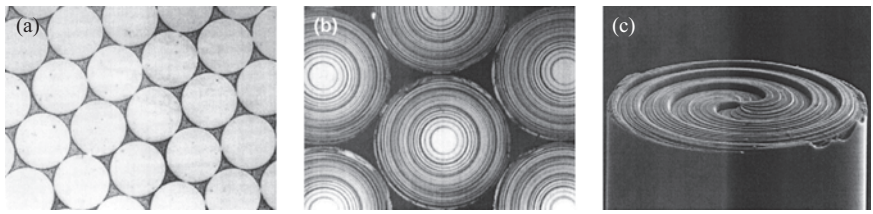

Figure 11.30 (a) Microscope image of a fiber bundle wafer polished and ready for lithographic processing; (b) diffractive lenses fabricated on the wafer; (c) an element with multiplexed collimation and vortex phase functions fabricated on the end facet of an individual fiber rod [331].

The lithographic methods described above generally suffer from severely limited throughput as the process is carried out sequentially on individual fibers. Attempts have been made to parallelize the fabrication. Johnson *et al*. stacked fibers into a bundle using epoxy adhesive, sliced the bundle, and polished the end facets to form thin wafers comprising short segments of fiber cores arrayed in a close-packed hexagonal lattice (Figure 11.30(a)) [331]. The wafers can then be processed following standard handling protocols of classical semiconductor wafers. Figure 11.30 illustrates optical diffractive lenses and an element combining collimation and vortex phase generation functions fabricated using this approach. It should be noted that the photomask used along the wafer has to be custom-made following the fabricated fiber array geometry to accommodate random defects in the fiber lattice.

Nanoimprint and its variants are also popular choices for subwavelength optics integration on fiber tips [332–336]. Batch processing of up to 40 fiber facets with feature resolution down to 15 nm was also demonstrated [337]. Figure 11.31(a) illustrates an embodiment of the process, which combines UV nanoimprint and nanotransfer to produce grating couplers attached to a fiber facet [338]. A mold containing the grating pattern was first etched in an SOI wafer. A gold film was subsequently deposited on the mold, followed by selective removal of gold on top of the mold using microcontact printing, leaving gold only in the trench lines. The fiber was then dipped into a UV-curable resist and actively aligned to the SOI grating before cross-linking the resist. As the gold pattern adheres to the resist much better than to SOI, separation of the fiber and the SOI grating resulted in transfer of the metallic grating onto the fiber facet. The grating-coupler-integrated fiber probe can deliver (or extract) light into (from) a planar waveguide once directly contacting the waveguide surface, potentially enabling nondestructive wafer-scale testing of photonic circuits.

Direct write techniques such as focused ion beam (FIB) milling and direct laser writing present another solution to circumvent the technical complications associated with handling of fiber facets in lithographic patterning. FIB milling has been applied to fiber-tip integration of nanoapertures [339], plasmonics nanostructures

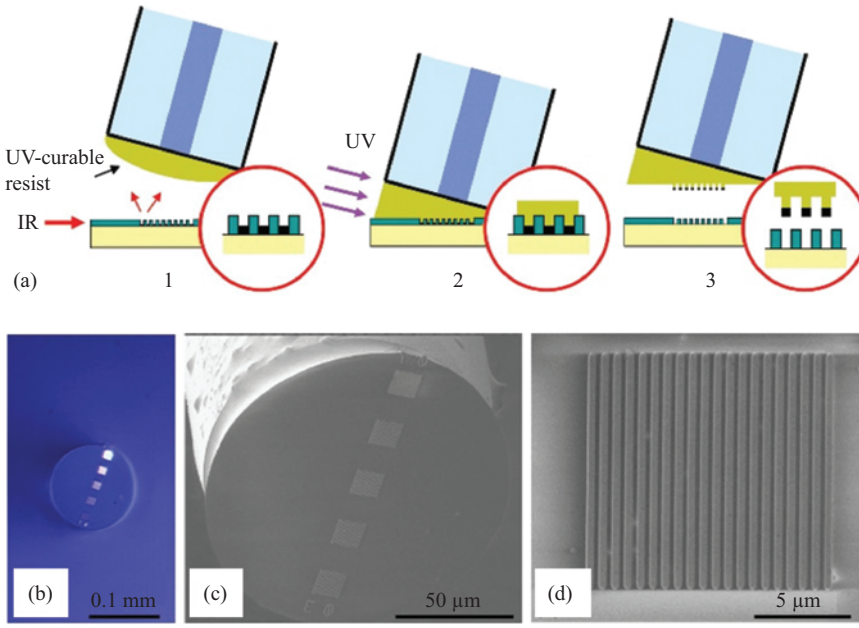

Figure 11.31 *(a) Schematic fabrication process of the grating-coupler-integrated fiber probe; (b) optical and (c) SEM micrographs of the fiber probe facet, showing the attached gratings; (d) top-view SEM image of the on-fiber grating coupler [338].*

[340,341], diffractive optical elements [342], photoacoustic sensors [343], as well as micro-channels for fluid filling in photonic crystal fibers [344]. FIB-etched surface corrugations can also be used as a template to define structures subsequently deposited on the fiber end facet [345]. It is worth pointing out that FIB milling inevitably causes contamination of the fiber by gallium ions, and thus the resulting fiber material optical property modification should be properly accounted for in the design phase [346,347].

Laser writing, in particular two-photo lithography or TPP, is uniquely poised for 3D optical structure fabrication on fiber facets with sub-micron alignment accuracy and resolution down to below 100 nm [348]. Single and compound micro-lenses [163,164], micro-prisms [165], phase masks [170], AFM probes [171], and photonic crystals (Figure 11.32) [168] are some examples of optical structures that have been integrated on optical fiber tips using TPP. Section 11.3.2.1 of this chapter provides further discussions about the technology for interested readers.

11.4 Summary and outlook

As the field of subwavelength optics continues to boom and novel nanophotonic device designs emerge (as other chapters in this book highlight), existing

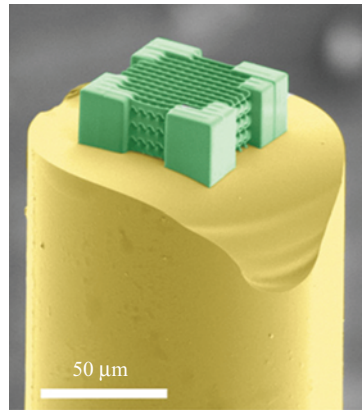

Figure 11.32 False-color SEM image of a woodpile photonic crystal fabricated on a fiber facet using TPP [168].

nanofabrication methods will continue to evolve and new technologies will surface to keep pace with the increasingly sophisticated demands. We foresee that the crossroads of ingenious nanophotonic designs and nanofabrication techniques will thrive as a leading source of inspiration for researchers aspiring to explore the field. In this spirit, it is the authors' hope that this chapter can serve as a convenient solution guide to both theorists and experimentalists who are exploring unconventional subwavelength structures. Finally, we hope that the discussions here can further inspire design and process innovations in the dynamic field of subwavelength optics, where 'there is plenty of room at the bottom' for both dancing angels and optical engineers alike.

References

[1] C. Zheng, *Nanofabrication: principles, capabilities and limits*. 2008.
[2] A. A. Tseng, *Nanofabrication: fundamentals and applications.* World Scientific, 2008.
[3] C. Papadopoulos, *Nanofabrication: principles and applications.* Springer, 2016.
[4] J. A. Liddle and G. M. Gallatin, "Nanomanufacturing: a perspective," *ACS Nano*, vol. 10, no. 3, pp. 2995–3014, 2016.
[5] D. G. Baranov, D. A. Zuev, S. I. Lepeshov, *et al*., "All-dielectric nanophotonics: the quest for better materials and fabrication techniques," *Optica*, vol. 4, no. 7, 2017.
[6] R. C. Devlin, M. Khorasaninejad, W. T. Chen, J. Oh, and F. Capasso, "Broadband high-efficiency dielectric metasurfaces for the visible spectrum," *Proc. Natl. Acad. Sci.*, vol. 113, no. 38, pp. 10473–10478, 2016.
[7] A. Y. Zhu, A. I. Kuznetsov, B. Luk'Yanchuk, N. Engheta, and P. Genevet, "Traditional and emerging materials for optical metasurfaces," *Nanophotonics*, vol. 6, no. 2, pp. 452–471, 2017.

[8] N. I. Zheludev and Y. S. Kivshar, "From metamaterials to metadevices," *Nat. Mater.*, vol. 11, no. 11, pp. 917–924, 2012.
[9] N. Meinzer, W. L. Barnes, and I. R. Hooper, "Plasmonic meta-atoms and metasurfaces," *Nat. Photonics*, vol. 8, no. 12, pp. 889–898, 2014.
[10] H.-T. Chen, A. J. Taylor, and N. Yu, "A review of metasurfaces: physics and applications," *Reports Prog. Phys.*, vol. 79, no. 7, p. 076401, 2016.
[11] A. M. Shaltout, A. V. Kildishev, and V. M. Shalaev, "Evolution of photonic metasurfaces: from static to dynamic," *J. Opt. Soc. Am. B*, vol. 33, no. 3, p. 501, 2016.
[12] M. Decker and I. Staude, "Resonant dielectric nanostructures: a low-loss platform for functional nanophotonics," *J. Opt.*, vol. 18, no. 103001, 2016.
[13] S. Walia, C. M. Shah, P. Gutruf, *et al*., "Flexible metasurfaces and metamaterials: a review of materials and fabrication processes at micro-and nanoscales," *Appl. Phys. Rev.*, vol. 2, no. 1, p. 11303, 2015.
[14] V.-C. Su, C. H. Chu, G. Sun, and D. P. Tsai, "Advances in optical metasurfaces: fabrication and applications [Invited]," *Opt. Express*, vol. 26, no. 10, p. 13148, 2018.
[15] A. She, S. Zhang, S. Shian, D. R. Clarke, and F. Capasso, "Large area metalenses: design, characterization, and mass manufacturing," *Opt. Express*, vol. 26, no. 2, p. 1573, 2018.
[16] P. Genevet, F. Capasso, F. Aieta, M. Khorasaninejad, and R. Devlin, "Recent advances in planar optics: from plasmonic to dielectric metasurfaces," *Optica*, vol. 4, no. 1, p. 139, 2017.
[17] P. Cheben, R. Halir, J. H. Schmid, H. A. Atwater, and D. R. Smith, "Subwavelength integrated photonics," *Nature*, vol. 560, no. 7720, pp. 565–572, 2018.
[18] L. Zhang, S. Mei, K. Huang, and C. W. Qiu, "Advances in full control of electromagnetic waves with metasurfaces," *Adv. Opt. Mater.*, vol. 4, no. 6, pp. 818–833, 2016.
[19] H.-H. Hsiao, C. H. Chu, and D. P. Tsai, "Fundamentals and applications of metasurfaces," *Small Methods*, vol. 1, no. 4, p. 1600064, 2017.
[20] N. Yu and F. Capasso, "Flat optics with designer metasurfaces," *Nat. Mater.*, vol. 13, no. 2, pp. 139–150, 2014.
[21] N. Yu, P. Genevet, M. A. Kats, *et al*., "Light propagation with phase discontinuities reflection and refraction," *Science*, vol. 334, no. 6054, pp. 333–337, 2011.
[22] E. Karimi, S. A. Schulz, I. De Leon, H. Qassim, J. Upham, and R. W. Boyd, "Generating optical orbital angular momentum at visible wavelengths using a plasmonic metasurface," *Light Sci. Appl.*, vol. 3, pp. 1–4, 2014.
[23] W. Cai, C. Jun, and J. White, "Plasmonics for extreme light concentration and manipulation," *Nat. Mater.*, vol. 9, no. 3, pp. 193–204, 2010.
[24] M. Pelton, J. Aizpurua, and G. Bryant, "Metal-nanoparticle plasmonics," *Laser Photon. Rev.*, vol. 2, no. 3, pp. 136–159, 2008.
[25] Y. Zhao and A. Alu, "Tailoring the dispersion of plasmonic nanorods to realize broadband optical meta-waveplates," *Nano Lett.*, vol. 13, 2013.

[26] K. Sarabandi and N. Behdad, "A frequency selective surface with miniaturized elements," *IEEE Trans. Antennas Propag.*, vol. 55, no. 5, pp. 1239–1245, 2007.

[27] P. Stute, S. Uniiwrsitj, and S. Collejie, "Flat lens antenna concept using aperture coupled microstrip patches," *Electron. Lett.*, vol. 32, no. 23, pp. 2109–2111, 1996.

[28] M. A. Al-Joumayly and N. Behdad, "A generalized method for synthesizing low-profile, band-pass frequency selective surfaces with non-resonant constituting elements," *IEEE Trans. Antennas Propag.*, vol. 58, no. 12, pp. 4033–4041, 2010.

[29] A. Boltasseva and H. A. Atwater, "Low-loss plasmonic metamaterials," *Science*, vol. 331, no. 6015, pp. 290–291, 2011.

[30] P. R. West, S. Ishii, G. V. Naik, N. K. Emani, V. M. Shalaev, and A. Boltasseva, "Searching for better plasmonic materials," *Laser Photon. Rev.*, vol. 4, no. 6, pp. 795–808, 2010.

[31] M. G. Blaber, M. D. Arnold, and M. J. Ford, "A review of the optical properties of alloys and intermetallics for plasmonics," *J. Phys. Condens. Matter*, vol. 22, no. 14, 2010.

[32] D. A. Bobb, G. Zhu, M. Mayy, *et al.*, "Engineering of low-loss metal for nanoplasmonic and metamaterials applications," *Appl. Phys. Lett.*, vol. 95, no. 15, p. 151102, 2009.

[33] M. Jablan, H. Buljan, and M. Soljačić, "Plasmonics in graphene at infrared frequencies," *Phys. Rev. B*, vol. 80, no. 24, p. 245435, 2009.

[34] S. A. Gregory, Y. Wang, C. H. De Groot, and O. L. Muskens, "Extreme subwavelength metal oxide direct and complementary metamaterials," *ACS Photonics*, vol. 2, pp. 606−614, 2015.

[35] S. Q. Li, P. Guo, L. Zhang, W. Zhou, T. W. Odom, and T. Seideman, "Infrared plasmonics with indium-tin-oxide nanorod arrays," *ACS Nano*, vol. 5, no. 11, pp. 9161–9170, 2011.

[36] M. Abb, Y. Wang, N. Papasimakis, C. H. De Groot, and O. L. Muskens, "Surface-enhanced infrared spectroscopy using metal oxide plasmonic antenna arrays," *Nano Lett.*, vol. 14, pp. 346−352, 2014.

[37] J. Kim, A. Dutta, B. Memarzadeh, A. V Kildishev, H. Mosallaei, and A. Boltasseva, "Zinc oxide based plasmonic multilayer resonator: localized and gap surface plasmon in the infrared," *ACS Photonics*, vol. 2, pp. 1224−1230, 2015.

[38] J. Park, J. Kang, S. J. Kim, X. Liu, and M. L. Brongersma, "Dynamic reflection phase and polarization control in metasurfaces," *Nano Lett.*, vol. 17, pp. 407−413, 2017.

[39] C. Rhodes, S. Franzen, J. P. Maria, *et al.*, "Surface plasmon resonance in conducting metal oxides," *J. Appl. Phys.*, vol. 100, no. 5, 2006.

[40] C. Rhodes, M. Cerruti, A. Efremenko, *et al.*, "Dependence of plasmon polaritons on the thickness of indium tin oxide thin films," *J. Appl. Phys.*, vol. 103, no. 9, 2008.

[41] K. Ellmer and R. Mientus, "Carrier transport in polycrystalline ITO and ZnO:Al II: the influence of grain barriers and boundaries," *Thin Solid Films*, vol. 516, no. 17, pp. 5829–5835, 2008.

[42] F. Lai, L. Lin, R. Gai, Y. Lin, and Z. Huang, "Determination of optical constants and thicknesses of In_2O_3:Sn films from transmittance data," *Thin Solid Films*, vol. 515, no. 18, pp. 7387–7392, 2007.

[43] M. Lv, X. Xiu, Z. Peng, *et al*., "Structural, electrical and optical properties of zirconium-doped zinc oxide films prepared by radio frequency magnetron sputtering," *Thin Solid Films*, vol. 516, no. 8, pp. 2017–2021, 2008.

[44] J. G. Lu, Z. Z. Ye, Y. J. Zheng, *et al*., "Structural, optical, and electrical properties of (Zn,Al)O films over a wide range of compositions," *J. Appl. Phys.*, vol. 100, no. 7, p. 073714, 2006.

[45] J. Kim, S. Choudhury, C. Devault, *et al*., "Controlling the polarization state of light with plasmonic metal oxide metasurface," *ACS Nano*, vol. 10, pp. 9326−9333, 2016.

[46] S. Jahani and Z. Jacob, "All-dielectric metamaterials," *Nat. Nanotechnol*., vol. 11, no. 1, pp. 23–36, 2016.

[47] A. I. Kuznetsov, A. E. Miroshnichenko, M. L. Brongersma, Y. S. Kivshar, and B. Luk'yanchuk, "Optically resonant dielectric nanostructures," *Science*, vol. 354, no. 6314, p. aag2472, 2016.

[48] A. Arbabi, Y. Horie, A. J. Ball, M. Bagheri, and A. Faraon, "Subwavelength-thick lenses with high numerical apertures and large efficiency based on high contrast transmitarrays," *Nat. Commun.*, vol. 6, no. pp. 1–10, 2015.

[49] L. Zhang, J. Ding, H. Zheng, *et al*., "Huygens meta-optics," *Nat. Commun.*, no. 2018, pp. 1–9.

[50] I. Staude and J. Schilling, "Metamaterial-inspired silicon nanophotonics," *Nat. Photonics*, vol. 11, no. 5, pp. 274–284, 2017.

[51] M. Decker, I. Staude, M. Falkner, *et al*., "High-efficiency dielectric Huygens' surfaces," *Adv. Opt. Mater.*, vol. 3, no. 6, pp. 813–820, 2015.

[52] A. B. Evlyukhin, C. Reinhardt, and B. N. Chichkov, "Multipole light scattering by nonspherical nanoparticles in the discrete dipole approximation," *Phys. Rev. B - Condens. Matter Mater. Phys*., vol. 84, no. 23, pp. 1–8, 2011.

[53] E. Arbabi, A. Arbabi, S. M. Kamali, Y. Horie, M. S. Faraji-Dana, and A. Faraon, "MEMS-tunable dielectric metasurface lens," *Nat. Commun.*, vol. 9, no. 1, 2018.

[54] A. Arbabi, E. Arbabi, S. M. Kamali, Y. Horie, S. Han, and A. Faraon, "Miniature optical planar camera based on a wide-angle metasurface doublet corrected for monochromatic aberrations," *Nat. Commun.*, vol. 7, pp. 1–31, 2016.

[55] P. Spinelli, M. A. Verschuuren, and A. Polman, "Broadband omnidirectional antireflection coating based on subwavelength surface Mie resonators," *Nat. Commun.*, vol. 3, pp. 692–695, 2012.

[56] C. Shane, Z. Alan, B. Elyas, *et al*., "Broadband transparent and CMOS-compatible flat optics with silicon nitride metasurfaces [Invited]," *Opt. Mater. Express*, vol. 8, no. 8, p. 2330, 2018.

[57] S. Colburn, A. Zhan, and A. Majumdar, "Metasurface optics for full-color computational imaging," *Sci. Adv.*, vol. 4, no. 2114, pp. 1–7, 2018.
[58] A. Zhan, S. Colburn, R. Trivedi, T. K. Fryett, C. M. Dodson, and A. Majumdar, "Low-contrast dielectric metasurface optics," *ACS Photonics*, vol. 3, pp. 1–6, 2016.
[59] G. E. Jettison, "Optical functions of GaAs, GaP, and Ge determined by two-channel polarization modulation ellipsometry," *Opt. Mater. (Amst)*., pp. 151–160, 1992.
[60] S. Liu, M. B. Sinclair, S. Saravi, *et al*., "Resonantly enhanced second-harmonic generation using III−V semiconductor all-dielectric metasurfaces sheng," *Nano Lett.*, vol. 16, pp. 5426–5432, 2016.
[61] M. R. Shcherbakov, S. Liu, V. V. Zubyuk, *et al*., "Ultrafast all-optical tuning of direct-gap semiconductor metasurfaces maxim," *Nat. Commun.*, vol. 8, pp. 1–5, 2017.
[62] S. Liu, G. A. Keeler, J. L. Reno, M. B. Sinclair, and I. Brener, "III–V semiconductor nanoresonators—a new strategy for passive, active, and nonlinear all-dielectric metamaterials," *Adv. Opt. Mater.*, vol. 4, no. 10, pp. 1457–1462, 2016.
[63] S. Person, M. Jain, Z. Lapin, J. Jose, G. Wicks, and L. Novotny, "Demonstration of zero optical backscattering from single nanoparticles," *Nano Lett.*, vol. 13, pp. 1806−1809, 2013.
[64] W. T. Chen, A. Y. Zhu, V. Sanjeev, *et al*., "A broadband achromatic metalens for focusing and imaging in the visible," *Nat. Nanotechnol.*, vol. 13, no. 3, pp. 220–226, 2018.
[65] L. Li, H. Lin, Y. Huang, *et al*., "High-performance flexible waveguide-integrated photodetectors," *Optica*, vol. 5, no. 1, pp. 44–51, 2018.
[66] J. Hu, L. Li, H. Lin, P. Zhang, W. Zhou, and Z. Ma, "Flexible integrated photonics: where materials, mechanics and optics meet [Invited]," *Opt. Mater. Express*, vol. 3, no. 9, pp. 1313–1331, 2013.
[67] L. Li, H. Lin, S. Qiao, *et al*., "Integrated flexible chalcogenide glass photonic devices," *Nat. Photonics*, vol. 8, no. 8, pp. 643–649, 2014.
[68] J. Hu, L. Li, H. Lin, *et al*., "Chalcogenide glass microphotonics: stepping into the spotlight," *Am. Ceram. Soc. Bull.*, vol. 94, no. 4, pp. 24–29, 2015.
[69] L. Li, H. Lin, S. Qiao, *et al*., "Monolithically integrated stretchable photonics," *Light Sci. Appl.*, vol. 7, no. 2, p. 17138, 2018.
[70] Q. Du, Y. Huang, J. Li, *et al*., "Low-loss photonic device in Ge – Sb – S chalcogenide glass," *Opt. Lett.*, vol. 41, no. 13, pp. 3090–3093, 2016.
[71] M. Wuttig, H. Bhaskaran, and T. Taubner, "Phase-change materials for non-volatile photonic applications," *Nat. Publ. Gr.*, vol. 11, no. 8, pp. 465–476, 2017.
[72] J. C. Ginn, I. Brener, D. W. Peters, *et al*., "Realizing optical magnetism from dielectric metamaterials," *Phys. Rev. Lett.*, vol. 108, no. 097402, pp. 1–5, 2012.
[73] S. Liu, M. B. Sinchair, T. S. Mahony, *et al*., "Optical magnetic mirrors without metals," *Optica*, vol. 1, no. 4, p. 250, 2014.

[74] S. Liu, J. F. Ihlefeld, J. Dominguez, *et al*., "Realization of tellurium-based all dielectric optical metamaterials using a multi-cycle deposition-etch process," *Appl. Phys. Lett.*, vol. 102, no. 16, p. 161905, 2013.
[75] T. Lewi, H. A. Evans, N. A. Butakov, and J. A. Schuller, "Ultrawide thermo-optic tuning of PbTe meta-atoms," *Nano Lett.*, vol. 17, no. 6, p. 3940, 2017.
[76] L. Zhang, J. Ding, H. Zheng, *et al*., "Ultra-thin high-efficiency mid-infrared transmissive Huygens meta-optics," *Nat. Commun.*, vol. 9, no. 1, p. 1481, 2018.
[77] J. Wang, J. Hu, X. Sun, *et al*., "Structural, electrical, and optical properties of thermally evaporated nanocrystalline PbTe films," *J. Appl. Phys.*, vol. 104, no. 5, p. 053707, 2008.
[78] J. Wang, J. Hu, P. Becla, A. M. Agarwal, and L. C. Kimerling, "Resonant-cavity-enhanced mid-infrared photodetector on a silicon platform," *Opt. Express*, vol. 18, no. 12, pp. 12890–12896, 2010.
[79] J. Wang, T. Zens, J. Hu, P. Becla, L. C. Kimerling, and A. M. Agarwal, "Monolithically integrated, resonant-cavity-enhanced dual-band mid-infrared photodetector on silicon," *Appl. Phys. Lett.*, vol. 100, no. 21, p. 211106, 2012.
[80] Z. Han, V. Singh, D. Kita, *et al*., "On-chip chalcogenide glass waveguide-integrated mid-infrared PbTe detectors," *Appl. Phys. Lett.*, vol. 109, no. 7, p. 071111, 2016.
[81] Q. Wang, E. T. F. Rogers, B. Gholipour, *et al*., "Optically reconfigurable metasurfaces and photonic devices based on phase change materials," *Nat. Photonics*, vol. 10, no. 1, pp. 60–65, 2015.
[82] A. Tittl, A.-K. U. Michel, M. Schäferling, *et al*., "A switchable mid-infrared plasmonic perfect absorber with multispectral thermal imaging capability," *Adv. Mater.*, vol. 27, pp. 4597–4603, 2015.
[83] A. Karvounis, B. Gholipour, K. F. MacDonald, and N. I. Zheludev, "All-dielectric phase-change reconfigurable metasurface," *Appl. Phys. Lett.*, vol. 109, no. 5, 2016.
[84] C. H. Chu, M. L. Tseng, J. Chen, *et al*., "Active dielectric metasurface based on phase-change medium," *Laser Photonics Rev*, vol. 10, no. 6, 2016.
[85] X. Luo, M. Hong, and S. A. Maier, "Engineering the phase front of light with phase-change material based planar lenses," *Sci. Rep*., vol. 5, no. 8660, pp. 1–7, 2015.
[86] X. Yin, T. Steinle, L. Huang, *et al*., "Beam switching and bifocal zoom lensing using active plasmonic metasurfaces," *Light Sci. Appl.*, vol. 6, no. 7, p. e17016, 2017.
[87] Y. G. Chen, T. S. Kao, B. Ng, *et al*., "Hybrid phase-change plasmonic crystals for active tuning of lattice resonances," *Opt. Express*, vol. 21, no. 11, pp. 1566–1569, 2013.
[88] Y. Zhang, J. B. Chou, J. Li, *et al*., "Broadband transparent optical phase change materials for high-performance nonvolatile photonics," *Nat. Commun.*, vol. 10, no. 4279, pp. 1–9, 2019.
[89] K. Liu, S. Lee, S. Yang, O. Delaire, and J. Wu, "Recent progresses on physics and applications of vanadium dioxide," *Mater. Today*, vol. 21, no. 8, pp. 875–896, 2018.

[90] H. Kocer, S. Butun, B. Banar, *et al*., "Thermal tuning of infrared resonant absorbers based on hybrid gold-VO_2 nanostructures," *Appl. Phys. Lett.*, vol. 106, 2015.
[91] K. Dong, S. Hong, Y. Deng, *et al*., "A lithography-free and field-programmable photonic metacanvas," *Adv. Mater.*, vol. 30, 2018.
[92] Y. Ke, X. Wen, D. Zhao, R. Che, Q. Xiong, and Y. Long, "Controllable fabrication of two-dimensional patterned VO_2 nanoparticle, nanodome, and nanonet arrays with tunable temperature-dependent localized surface plasmon resonance," *ACS Nano*, vol. 11, pp. 7542−7551, 2017.
[93] J. Rensberg, S. Zhang, Y. Zhou, *et al*., "Active optical metasurfaces based on defect-engineered phase-transition materials," *Nano Lett.*, vol. 16, pp. 1050−1055, 2016.
[94] O. L. Muskens, L. Bergamini, Y. Wang, *et al*., "Antenna-assisted picosecond control of nanoscale phase transition in vanadium dioxide," *Light Sci. Appl.*, vol. 5, no. e16173-9, 2016.
[95] G. Kaplan, K. Aydin, and J. Scheuer, "Dynamically controlled plasmonic nano-antenna phased array utilizing vanadium dioxide [Invited]," *Opt. Mater. Express*, vol. 5, no. 11, pp. 2457–2463, 2015.
[96] S. K. Earl, T. D. James, T. J. Davis, *et al*., "Tunable optical antennas enabled by the phase transition in vanadium dioxide," *Opt. Express*, vol. 21, no. 22, pp. 27503–27508, 2013.
[97] A. U. Michel, W. W. Tobias, T. Taubner, *et al*., "Using low-loss phase-change materials for mid-infrared antenna resonance tuning," *Nano Lett.*, vol. 13, pp. 3470−3475, 2013.
[98] S. K. Earl, T. D. James, D. E. Gómez, R. E. Marvel, and R. F. Haglund, "Switchable polarization rotation of visible light using a plasmonic metasurface," *APL Photonics*, vol. 2, no. 016103, 2017.
[99] F. Ligmajer, L. Kejik, U. Tiwari, *et al*., "Epitaxial VO_2 nanostructures: a route to large-scale, switchable dielectric metasurfaces," *ACS Photonics*, vol. 5, pp. 2561−2567, 2018.
[100] H. Lin, Y. Song, Y. Huang, *et al*., "Chalcogenide glass-on-graphene photonics," *Nat. Photonics*, vol. 11, pp. 798–805, 2017.
[101] L. Ju, B. Geng, J. Horng, *et al*., "Graphene plasmonics for tunable terahertz metamaterials," *Nat. Nanotechnol.*, vol. 6, no. 10, pp. 630–634, 2011.
[102] A. N. Grigorenko, M. Polini, and K. S. Novoselov, "Graphene plasmonics," *Nat. Photonics*, vol. 6, 2012.
[103] F. Withers, O. D. Pozo-Zamudio, A. Mishchenko, *et al*., "Light-emitting diodes by band-structure engineering in van der Waals heterostructures," *Nat. Mater.*, vol. 14, no. 3, pp. 301–306, 2015.
[104] Z. Sun, A. Martinez, and F. Wang, "Optical modulators with 2D layered materials," *Nat. Photonics*, vol. 10, no. 4, pp. 227–238, 2016.
[105] M. Liu, X. Ying, E. Ulin-Avila, *et al*., "A graphene-based broadband optical modulator," *Nature*, vol. 474, no. 7349, pp. 64–67, 2011.

[106] Y. Yao, R. Shankar, M. A. Kats, *et al*., "Electrically tunable metasurface perfect absorbers for ultrathin mid-infrared optical modulators," *Nano Lett.*, vol. 14, pp. 6526−6532, 2014.

[107] V. W. Brar, M. S. Jang, M. Sherrott, J. J. Lopez, and H. A. Atwater, "Highly confined tunable mid-infrared plasmonics in graphene nanoresonators," *Nano Lett.*, vol. 13, no. 6, pp. 2541–2547, 2013.

[108] S. Thongrattanasiri, F. H. L. Koppens, and F. J. García De Abajo, "Complete optical absorption in periodically patterned graphene," *Phys. Rev. Lett.*, vol. 108, no. 4, pp. 1–5, 2012.

[109] Z. Fei, A. S. Rodin, G. O. Andreev, *et al*., "Gate-tuning of graphene plasmons revealed by infrared nano-imaging," *Nature*, vol. 486, no. 7405, pp. 82–85, 2012.

[110] F. Bonaccorso, Z. Sun, T. Hasan, and A. C. Ferrari, "Graphene photonics and optoelectronics," *Nat. Photonics*, vol. 4, pp. 611–622, 2010.

[111] X. Gan, R. J. Shiue, Y. Gao, *et al*., "Chip-integrated ultrafast graphene photodetector with high responsivity," *Nat. Photonics*, vol. 7, no. 11, pp. 883–887, 2013.

[112] Y. Hu, M. Pantouvaki, J. V. Campenhout, *et al*., "Broadband 10 Gb/s operation of graphene electro-absorption modulator on silicon," *Laser Photonics Rev*., vol. 10, no. 2, pp. 307–316, 2016.

[113] L. O. Nyakiti, V. D. Wheeler, N. Y. Garces, R. L. Myers-Ward, C. R. Eddy, and D. K. Gaskill, "Enabling graphene-based technologies: toward wafer-scale production of epitaxial graphene," *MRS Bull.*, vol. 37, no. 12, pp. 1149–1157, 2012.

[114] C. C. Huang, F. Al-Saab, Y. Wang, *et al*., "Scalable high-mobility MoS_2 thin films fabricated by an atmospheric pressure chemical vapor deposition process at ambient temperature," *Nanoscale*, vol. 6, no. 21, pp. 12792–12797, 2014.

[115] L. Zhou, K. Xu, A. Zubair, *et al*., "Large-area synthesis of high-quality uniform few-layer $MoTe_2$," *J. Am. Chem. Soc.*, vol. 137, no. 37, pp. 11892–11895, 2015.

[116] L. Colombo, R. M. Wallace, and R. S. Ruoff, "Graphene growth and device integration," *Proc. IEEE*, vol. 101, no. 7, pp. 1536–1556, 2013.

[117] B. Lee, G. Mordi, M. J. Kim, *et al*., "Characteristics of high-k Al_2O_3 dielectric using ozone-based atomic layer deposition for dual-gated graphene devices," *Appl. Phys. Lett.*, vol. 97, no. 4, pp. 2008–2011, 2010.

[118] J. R. Williams, L. DiCarlo, and C. M. Marcus, "Quantum Hall effect in a gate-controlled p-n junction of graphene," *Science*, vol. 317, no. 5838, pp. 638–641, 2007.

[119] X. Wang, S. M. Tabakman, and H. Dai, "Atomic layer deposition of metal oxides on pristine and functionalized graphene," *J. Am. Chem. Soc.*, vol. 130, no. 26, pp. 8152–8153, 2008.

[120] W. Zhu, D. Neumayer, V. Perebeinos, and P. Avouris, "Silicon nitride gate dielectrics and band gap engineering in graphene layers," *Nano Lett.*, vol. 10, no. 9, pp. 3572–3576, 2010.

[121] J. Proust, F. Bedu, S. Frédéric, *et al*., "Chemical alkaline etching of silicon Mie particles," *Adv. Opt. Mater.*, vol. 3, no. 9, pp. 1280–1286, 2015.
[122] S. Shrestha, A. C. Overvig, M. Lu, A. Stein, and N. Yu, "Broadband achromatic dielectric metalenses," *Light Sci. Appl.*, vol. 7, no. 1, 2018.
[123] S. Wang, P. C. Wu, V. C. Su, *et al*., "Broadband achromatic optical metasurface devices," *Nat. Commun.*, vol. 8, no. 1, pp. 1–9, 2017.
[124] E. Shkondin, O. Takayama, J. M. Lindhard, *et al*., "Fabrication of high aspect ratio TiO_2 and Al_2O_3 nanogratings by atomic layer deposition," *J. Vac. Sci. Technol. A Vacuum, Surfaces, Film*., vol. 34, no. 3, p. 031605, 2016.
[125] O. Takayama, E. Shkondin, A. Bodganov, *et al*., "Midinfrared surface waves on a high aspect ratio nanotrench platform," *ACS Photonics*, vol. 4, no. 11, pp. 2899–2907, 2017.
[126] T. M. Babinec, B. J. M. Hausmann, M. Khan, *et al*., "A diamond nanowire single-photon source," *Nat. Nanotechnol*., vol. 5, no. 3, pp. 195–199, 2010.
[127] R. Chikkaraddy, B. de Nijs, F. Benz, *et al*., "Single-molecule strong coupling at room temperature in plasmonic nanocavities," *Nature*, vol. 535, no. 7610, pp. 127–130, 2016.
[128] S. Lee, B. Park, J. S. Kim, and T. Il Kim, "Designs and processes toward high-aspect-ratio nanostructures at the deep nanoscale: unconventional nanolithography and its applications," *Nanotechnology*, vol. 27, no. 47, pp. 1–15, 2016.
[129] R. Micheloni, L. Crippa, C. Zambelli, and P. Olivo, "Architectural and integration options for 3D NAND flash memories," *Computers*, vol. 6, no. 3, p. 27, 2017.
[130] J. W. Coburn and H. F. Winters, "Ion- and electron-assisted gas-surface chemistry—an important effect in plasma etching," *J. Appl. Phys.*, vol. 50, no. 5, pp. 3189–3196, 1979.
[131] J. P. Simko, "Removal of fluorocarbon residues on CF_4/H_2 reactive-ion-etched silicon surfaces using a hydrogen plasma," *J. Electrochem. Soc.*, vol. 138, no. 1, p. 277, 1991.
[132] S. Bouchoule, R. Chanson, A. Pageau, *et al*., "Surface chemistry of InP ridge structures etched in Cl_2-based plasma analyzed with angular XPS," *J. Vac. Sci. Technol. A Vacuum, Surfaces, Film.*, vol. 33, no. 5, p. 05E124, 2015.
[133] V. M. Donnelly and A. Kornblit, "Plasma etching: yesterday, today, and tomorrow," *J. Vac. Sci. Technol. A Vacuum, Surfaces, Film*., vol. 31, no. 5, p. 050825, 2013.
[134] A. Arbabi, Y. Horie, M. Bagheri, and A. Faraon, "Dielectric metasurfaces for complete control of phase and polarization with subwavelength spatial resolution and high transmission," *Nat. Nanotechnol.*, vol. 10, no. 11, pp. 937–943, 2015.
[135] K. Grigoras, L. Sainiemi, J. Tiilikainen, A. Säynätjoki, V. M. Airaksinen, and S. Franssila, "Application of ultra-thin aluminum oxide etch mask made by atomic layer deposition technique," *J. Phys. Conf. Ser.*, vol. 61, no. 1, pp. 369–373, 2007.

[136] A. A. High, R. C. Devlin, A. Dibos, *et al*., "Visible-frequency hyperbolic metasurface," *Nature*, vol. 522, no. 7555, pp. 192–196, 2015.

[137] X. Chen, H. R. Park, M. Pelton, *et al*., "Atomic layer lithography of wafer-scale nanogap arrays for extreme confinement of electromagnetic waves," *Nat. Commun.*, vol. 4, pp. 1–7, 2013.

[138] K. Peng, J. Hu, Y. Yan, *et al*., "Fabrication of single-crystalline silicon nanowires by scratching a silicon surface with catalytic metal particles," *Adv. Funct. Mater.*, vol. 16, no. 3, pp. 387–394, 2006.

[139] K. Peng, H. Fang, J. Hu, *et al*., "Metal-particle-induced, highly localized site-specific etching of Si and formation of single-crystalline Si nanowires in aqueous fluoride solution," *Chem. — A Eur. J.*, vol. 12, no. 30, pp. 7942–7947, 2006.

[140] K. Balasundaram, J. S. Sadhu, J. C. Shin, *et al*., "Porosity control in metal-assisted chemical etching of degenerately doped silicon nanowires," *Nanotechnology*, vol. 23, no. 30, p. 305304, 2012.

[141] X. Li, "Metal assisted chemical etching for high aspect ratio nanostructures: a review of characteristics and applications in photovoltaics," *Curr. Opin. Solid State Mater. Sci.*, vol. 16, no. 2, pp. 71–81, 2012.

[142] H. Li, T. Ye, L. Shi, and C. Xie, "Fabrication of ultra-high aspect ratio (>160:1) silicon nanostructures by using Au metal assisted chemical etching," *J. Micromechanics Microengineering*, vol. 27, no. 12, p. 124002, 2017.

[143] C. Chang and A. Sakdinawat, "Ultra-high aspect ratio high-resolution nanofabrication for hard X-ray diffractive optics," *Nat. Commun.*, vol. 5, pp. 1–7, 2014.

[144] S. H. Kim, P. K. Mohseni, Y. Song, T. Ishihara, and X. Li, "Inverse metal-assisted chemical etching produces smooth high aspect ratio InP nanostructures," *Nano Lett.*, vol. 15, no. 1, pp. 641–648, 2015.

[145] J. D. Kim, M. Kim, L. Kong, *et al*., "Self-anchored catalyst interface enables ordered via array formation from submicrometer to millimeter scale for polycrystalline and single-crystalline silicon," *ACS Appl. Mater. Interfaces*, vol. 10, no. 10, pp. 9116–9122, 2018.

[146] K. Balasundaram, P. K. Mohseni, Y.-C. Shuai, D. Zhao, W. Zhou, and X. Li, "Photonic crystal membrane reflectors by magnetic field-guided metal-assisted chemical etching," *Appl. Phys. Lett.*, vol. 103, no. 21, p. 214103, 2013.

[147] H. D. Um, N. Kim, K. Lee, *et al*., "Versatile control of metal-assisted chemical etching for vertical silicon microwire arrays and their photovoltaic applications," *Sci. Rep.*, vol. 5, no. pp. 1–11, 2015.

[148] R. Divan, D. Rosenthal, K. Ogando, L. E. Ocola, D. Rosenmann, and N. Moldovan, "Metal-assisted etching of silicon molds for electroforming," *J. Vac. Sci. Technol. B, Nanotechnol. Microelectron. Mater. Process. Meas. Phenom.*, vol. 31, no. 6, p. 06FF03, 2013.

[149] K. Lee, D. Yang, S. H. Park, and R. H. Kim, "Review recent developments in the use of two-photon polymerization in precise 2D and 3D microfabrications," *Polym. Adv. Technol.*, vol. 17, no. 2, pp. 72–82, 2006.

[150] K. Satoshi, S. Hong-Bo, T. Tomokazu, and T. Kenji, "Finer features for functional microdevices," *Nature*, vol. 412, pp. 697–698, 2001.
[151] X. Z. Dong, Z. S. Zhao, and X. M. Duan, "Improving spatial resolution and reducing aspect ratio in multiphoton polymerization nanofabrication," *Appl. Phys. Lett.*, vol. 92, no. 9, pp. 90–93, 2008.
[152] D. Tan, Y. Li, F. Qi, *et al*., "Reduction in feature size of two-photon polymerization using SCR500," *Appl. Phys. Lett.*, vol. 90, no. 7, pp. 1–4, 2007.
[153] X. Zhou, Y. Hou, and J. Lin, "A review on the processing accuracy of two-photon polymerization," *AIP Adv.*, vol. 5, no. 3, p. 030701, 2015.
[154] H. Sun, T. Suwa, K. Takada, *et al*., "Shape precompensation in two-photon laser nanowriting of photonic lattices," *Appl. Phys. Lett.*, vol. 85, no. 17, pp. 3708–3710, 2004.
[155] C. Y. Liao, M. Bouriauand, P. L. Baldeck, J. C. Ĺon, Ć. Masclet, and T. T. Chung, "Two-dimensional slicing method to speed up the fabrication of micro-objects based on two-photon polymerization," *Appl. Phys. Lett.*, vol. 91, no. 3, pp. 1–4, 2007.
[156] D. Y. Yang, S. H. Park, T. W. Lim, *et al*., "Ultraprecise microreproduction of a three-dimensional artistic sculpture by multipath scanning method in two-photon photopolymerization," *Appl. Phys. Lett.*, vol. 90, no. 1, pp. 2005–2008, 2007.
[157] K. Takada, H. B. Sun, and S. Kawata, "Improved spatial resolution and surface roughness in photopolymerization- based laser nanowriting," *Appl. Phys. Lett.*, vol. 86, no. 7, pp. 1–3, 2005.
[158] S. H. Park, S. H. Lee, D. Y. Yang, H. J. Kong, and K. S. Lee, "Subregional slicing method to increase three-dimensional nanofabrication efficiency in two-photon polymerization," *Appl. Phys. Lett.*, vol. 87, no. 15, pp. 1–3, 2005.
[159] R. Guo, S. Xiao, X. Zhai, J. Li, A. Xia, and W. Huang, "Micro lens fabrication by means of femtosecond two photon photopolymerization," *Opt. Express*, vol. 14, no. 2, p. 810, 2006.
[160] D. Wu, S. Z. Wu, L. G. Niu, *et al*., "High numerical aperture microlens arrays of close packing," *Appl. Phys. Lett.*, vol. 97, no. 3, 2010.
[161] P. I. Dietrich, M. Blaicher, I. Reuter, *et al*., "In situ 3D nanoprinting of free-form coupling elements for hybrid photonic integration," *Nat. Photonics*, vol. 12, no. 4, pp. 241–247, 2018.
[162] J. Serbin, A. Egbert, A. Ostendorf, and B. N. Chichkov, "Femtosecond laser-induced two-photon polymerization of inorganic—organic hybrid materials for applications in photonics," *Opt. Lett.*, vol. 28, no. 5, pp. 301–303, 2003.
[163] T. Gissibl, S. Thiele, A. Herkommer, and H. Giessen, "Two-photon direct laser writing of ultracompact multi-lens objectives," *Nat. Photonics*, vol. 10, no. 8, p. 554, 2016.
[164] C. Liberale, G. Cojoc, P. Candeloro, *et al*., "Micro-optics fabrication on top of optical fibers using two-photon lithography," *IEEE Photonics Technol. Lett.*, vol. 22, no. 7, pp. 474–476, 2010.

[165] C. Liberale, G. Cojoc, F. Bragheri, *et al*., "Integrated microfluidic device for single-cell trapping and spectroscopy," *Sci. Rep.*, vol. 3, p. 1258, 2013.

[166] S. Thiele, A. Herkommer, H. Giessen, and T. Gissibl, "Sub-micrometre accurate free-form optics by three-dimensional printing on single-mode fibre," *Nat. Commun.*, vol. 7, pp. 1–9, 2016.

[167] M. Deubel, G. von Freymann, M. Wegener, S. Pereira, K. Busch, and C. M. Soukoulis, "Direct laser writing of three-dimensional photonic-crystal templates for telecommunications," *Nat. Mater.*, vol. 3, no. 7, pp. 444–447, 2004.

[168] H. E. Williams, D. J. Freppon, S. M. Kuebler, R. C. Rumpf, and M. A. Melino, "Fabrication of three-dimensional micro-photonic structures on the tip of optical fibers using SU-8," *Opt. Express*, vol. 19, no. 23, pp. 22910–22922, 2011.

[169] C. Jain, A. Braun, J. Gargiulo, B. Jang, G. Li, and H. Lehmann, "Hollow core light cage: Trapping light behind bars," *ACS Photonics*, 2018.

[170] T. Gissibl, M. Schmid, and H. Giessen, "Spatial beam intensity shaping using phase masks on single-mode optical fibers fabricated by femtosecond direct laser writing," *Optica*, vol. 3, no. 4, pp. 448–451, 2016.

[171] B. J. Jung, H. J. Kong, Y. H. Cho, *et al*., "Fabrication of sharp-needled conical polymer tip on the cross-section of optical fiber via two-photon polymerization for tuning-fork-based atomic force microscopy," *Opt. Commun.*, vol. 286, pp. 197–203, 2013.

[172] C. Lu and R. H. Lipson, "Interference lithography: a powerful tool for fabricating periodic structures," *Laser Photon. Rev.*, vol. 4, no. 4, pp. 568–580, 2009.

[173] S. R. J. Brueck, "Optical and interferometric lithography - nanotechnology enablers," *Proc. IEEE*, vol. 93, no. 10, pp. 1704–1721, 2005.

[174] C. Moormann, J. Bolten, and H. Kurz, "Spatial phase-locked combination lithography for photonic crystal devices," *Microelectron. Eng.*, vol. 74, pp. 417–422, 2004.

[175] I. Divliansky, T. S. Mayer, K. S. Holliday, and V. H. Crespi, "Fabrication of three-dimensional polymer photonic crystal structures using single diffraction element interference lithography," *Appl. Phys. Lett.*, vol. 82, no. 11, pp. 1667–1669, 2003.

[176] M. Campbell, D. N. Sharp, M. T. Harrison, and R. G. Denning, "Fabrication of photonic crystals for the visible spectrum by holographic lithography," *Nature*, vol. 404, no. 2, pp. 53–56, 2000.

[177] S. Yang, M. Megens, J. Aizenberg, P. Wiltzius, P. M. Chaikin, and W. B. Russel, "Creating periodic three-dimensional structures by multibeam interference of visible laser," *Chem. Mater.*, vol. 14, no. 7, pp. 2001–2003, 2002.

[178] F. Quiñónez, J. W. Menezes, and L. Cescato, "Band gap of hexagonal 2D photonic crystals with elliptical holes recorded by interference lithography," *Opt. Express*, vol. 14, no. 11, pp. 4873–4879, 2006.

[179] H. H. Solak, C. David, J. Gobrecht, *et al*., "Multiple-beam interference lithography with electron beam written gratings," *J. Vac. Sci. Technol. B*, vol. 20, no. 6, 2002.

[180] S. Yang, M. Megens, J. Aizenberg, P. Wiltzius, P. M. Chaikin, and W. B. Russel, "Creating periodic three-dimensional structures by multibeam interference of visible laser," *Chem. Mater.*, vol. 14, no. 7, pp. 2831–2833, 2002.

[181] O. Toader, T. Y. M. Chan, and S. John, "Photonic band gap architectures for holographic lithography," *Phys. Rev. Lett.*, vol. 92, no. 4, p. 4, 2004.

[182] Y. Lin, D. Rivera, Z. Poole, and K. P. Chen, "Five-beam interference pattern controlled through phases and wave vectors for diamondlike photonic crystals," *Appl. Opt.*, vol. 45, no. pp. 7971–7976, 2006.

[183] T. Y. M. Chan, O. Toader, and S. John, "Photonic band-gap formation by optical-phase-mask lithography," *Phys. Rev. E - Stat. Nonlinear, Soft Matter Phys.*, vol. 73, no. 4, pp. 1–11, 2006.

[184] C. Lu, X. K. Hu, I. V. Mitchell, and R. H. Lipson, "Diffraction element assisted lithography: pattern control for photonic crystal fabrication," *Appl. Phys. Lett.*, vol. 86, no. 19, p. 193110, 2005.

[185] Y. V. Miklyaev, D. C. Meisel, A. Blanco, *et al.*, "Three-dimensional face-centered-cubic photonic crystal templates by laser holography: fabrication, optical characterization, and band-structure calculations," *Appl. Phys. Lett.*, vol. 82, no. 8, pp. 1284–1286, 2003.

[186] Z. Poole, D. Xu, K. P. Chen, I. Olvera, K. Ohlinger, and Y. Lin, "Holographic fabrication of three-dimensional orthorhombic and tetragonal photonic crystal templates using a diffractive optical element," *Appl. Phys. Lett.*, vol. 91, no. 25, pp. 1–4, 2007.

[187] Y. Lin, P. R. Herman, and K. Darmawikarta, "Design and holographic fabrication of tetragonal and cubic photonic crystals with phase mask: toward the mass-production of three-dimensional photonic crystals," *Appl. Phys. Lett.*, vol. 86, no. 7, pp. 1–3, 2005.

[188] A. Shishido, I. B. Diviliansky, I. C. Khoo, *et al.*, "Direct fabrication of two-dimensional titania arrays using interference photolithography," *Appl. Phys. Lett.*, vol. 79, no. 3332, pp. 10–13, 2001.

[189] I. B. Divliansky, A. Shishido, I. C. Khoo, *et al.*, "Fabrication of two-dimensional photonic crystals using interference lithography and electrodeposition of CdSe," *Appl. Phys. Lett.*, vol. 79, no. 3392, pp. 1–4, 2005.

[190] Y. Lin, P. R. Herman, and E. L. Abolghasemi, "Proposed single-exposure holographic fabrication of microsphere-type photonic crystals through phase-mask techniques," *J. Appl. Phys.*, vol. 97, no. 9, pp. 4–7, 2005.

[191] Y. Lin, A. Harb, D. Rodriguez, K. Lozano, D. Xu, and K. P. Chen, "Holographic fabrication of photonic crystals using multidimensional phase masks masks," *J. Appl. Phys.*, vol. 104, no. 113111, 2008.

[192] J. Xavier and J. Joseph, "Complex photonic lattices embedded with tailored intrinsic defects by a dynamically reconfigurable single step interferometric approach," *Appl. Phys. Lett.*, vol. 104, no. 8, 2014.

[193] M. Kumar and J. Joseph, "Generating a hexagonal lattice wave field with a gradient basis structure," *Opt. Lett.*, vol. 39, no. 8, p. 2459, 2014.

[194] S. Behera, M. Kumar, and J. Joseph, "Submicrometer photonic structure fabrication by phase spatial-light-modulator-based interference lithography," *Opt. Lett.*, vol. 41, no. 8, p. 1893, 2016.

[195] J. Li, Y. Liu, X. Xie, *et al*., "Fabrication of photonic crystals with functional defects by one-step holographic lithography," *Opt. Express*, vol. 16, no. 17, p. 12899, 2008.

[196] G. Zito, B. Piccirillo, E. Santamato, A. Marino, V. Tkachenko, and G. Abbate, "Two-dimensional photonic quasicrystals by single beam computer-generated holography," *Opt. Express*, vol. 16, no. 8, p. 5164, 2008.

[197] M. Kumar and J. Joseph, "Optical generation of a spatially variant two-dimensional lattice structure by using a phase only spatial light modulator," *Appl. Phys. Lett.*, vol. 105, no. 5, 2014.

[198] Y. J. Liu and X. W. Sun, "Electrically tunable two-dimensional holographic photonic crystal fabricated by a single diffractive element," *Appl. Phys. Lett.*, vol. 89, no. 17, pp. 1–4, 2006.

[199] D. B. Burckel, P. J. Resnick, P. S. Finnegan, M. B. Sinclair, and P. S. Davids, "Micrometer-scale fabrication of complex three dimensional lattice + basis structures in silicon," *Opt. Mater. Express*, vol. 5, no. 10, p. 2231, 2015.

[200] D. B. Burckel, J. R. Wendt, G. A. Ten Eyck, A. R. Ellis, I. Brener, and M. B. Sinclair, "Fabrication of 3D metamaterial resonators using self-aligned membrane projection lithography," *Adv. Mater.*, vol. 22, no. 29, pp. 3171–3175, 2010.

[201] D. B. Burckel, J. R. Wendt, G. A. T. Eyck, *et al*., "Micrometer-scale cubic unit cell 3D metamaterial layers," *Adv. Mater.*, vol. 22, no. 44, pp. 5053–5057, 2010.

[202] D. B. Burckel, S. Campione, P. S. Davids, and M. B. Sinclair, "Three dimensional metafilms with dual channel unit cells," *Appl. Phys. Lett.*, vol. 110, no. 14, p. 143107, 2017.

[203] D. B. Burckel, "Device-level and module-level three-dimensional integrated circuits created using oblique processing," *J. Micro/Nanolithography, MEMS, MOEMS*, vol. 15, no. 3, p. 34504, 2016.

[204] C. A. Mirkin, R. L. Letsinger, R. C. Mucic, and J. J. Storhoff, "A DNA-based method for rationally assembling nanoparticles into macroscopic materials," *Nature*, vol. 382, no. 6592, pp. 607–609, 1996.

[205] A. P. Alivisatos, K. P. Johnsson, X. Peng, *et al*., "Organization of nanocrystal molecules using DNA," *Nature*, vol. 382, no. 6592, pp. 609–611, 1996.

[206] X. Li, X. Yang, J. Qi, and N. C. Seeman, "Antiparallel DNA double crossover molecules as components for nanoconstruction," *J. Am. Chem. Soc.*, vol. 118, no. 26, pp. 6131–6140, 1996.

[207] S. Y. Park, A. K. R. Lytton-Jean, B. Lee, S. Weigand, G. C. Schatz, and C. A. Mirkin, "DNA-programmable nanoparticle crystallization," *Nature*, vol. 451, no. 7178, pp. 553–556, 2008.

[208] E. Auyeung, T. I. N. G. Li, A. J. Senesi, *et al*., "DNA-mediated nanoparticle crystallization into Wulff polyhedra," *Nature*, vol. 505, no. 7481, pp. 73–77, 2014.

[209] R. J. Macfarlane, B. Lee, M. R. Jones, N. Harris, G. C. Schatz and C. A. Mirkin "Supplementary info: nanoparticle superlattice engineering with DNA," *Science*, vol. 334, no. 6053, pp. 204–8, 2011.

[210] M. R. Jones, K. D. Osberg, R. J. MacFarlane, M. R. Langille, and C. A. Mirkin, "Templated techniques for the synthesis and assembly of plasmonic nanostructures," *Chem. Rev.*, vol. 111, no. 6, pp. 3736–3827, 2011.

[211] Z. H. Jiang, L. Kang, and D. H. Werner, "Conformal metasurface-coated dielectric waveguides for highly confined broadband optical activity with simultaneous low-visibility and reduced crosstalk," *Nat. Commun.*, vol. 8, no. 1, p. 356, 2017.

[212] S. M. Kamali, A. Arbabi, E. Arbabi, Y. Horie, and A. Faraon, "Decoupling optical function and geometrical form using conformal flexible dielectric metasurfaces," *Nat. Commun.*, vol. 7, p. 11618, 2016.

[213] J. Cheng, S. Jafar-Zanjani, and H. Mosallaei, "All-dielectric ultrathin conformal metasurfaces: lensing and cloaking applications at 532 nm wavelength," *Sci. Rep.*, vol. 6, p. 38440, 2016.

[214] D.-H. Kim, N. Lu, R. Ma, *et al*., "Epidermal electronics," *Science*, vol. 333, no. 6044, pp. 838–843, 2011.

[215] H. Zhao, K. O'Brien, S. Li, and R. F. Shepherd, "Optoelectronically innervated soft prosthetic hand via stretchable optical waveguides," *Sci. Robot.*, vol. 1, no. 1, p. eaai7529, 2016.

[216] S. Aikio, J. Hiltunen, J. Hiitola-Keinänen, *et al*., "Disposable photonic integrated circuits for evanescent wave sensors by ultra-high volume roll-to-roll method," *Opt. Express*, vol. 24, no. 3, pp. 2527–2541, 2016.

[217] S. Aikio, J. Hiltunen, Johanna Hiitola-Keinänen, *et al*., "Disposable (bio) chemical integrated optical waveguide sensors implemented on roll-to-roll produced platforms," *RSC Adv*., vol. 6, no. 56, pp. 50414–50422, 2016.

[218] C. L. Yu, H. Kim, N. De Leon, *et al*., "Stretchable photonic crystal cavity with wide frequency tunability," *Nano Lett.*, vol. 13, no. 1, pp. 248–252, 2012.

[219] M. L. Tseng, J. Yang, M. Semmlinger, C. Zhang, P. Nordlander, and N. J. Halas, "Two-dimensional active tuning of an aluminum plasmonic array for full-spectrum response," *Nano Lett.*, vol. 17, no. 10, pp. 6034–6039, 2017.

[220] W. Jinxiu, Z. Hongbo, C. Huanjun, Z. Weihong, and C. Jian, "Stretchable plasmonic substrate with tunable resonances for surface-enhanced Raman spectroscopy," *J. Opt.*, vol. 17, no. 11, p. 114015, 2015.

[221] H.-S. Ee and R. Agarwal, "Tunable metasurface and flat optical zoom lens on a stretchable substrate," *Nano Lett.*, vol. 16, no. 4, pp. 2818–2823, 2016.

[222] Y. Zou, L. Moreel, H. Lin, *et al*., "Solution processing and resist-free nanoimprint fabrication of thin film chalcogenide glass devices: inorganic-

organic hybrid photonic integration," *Adv. Opt. Mater.*, vol. 2, no. 8, pp. 759–764, 2014.

[223] A. She, S. Zhang, S. Shian, D. R. Clarke, and F. Capasso, "Adaptive metalenses with simultaneous electrical control of focal length, astigmatism, and shift," *Sci. Adv.*, vol. 4, no. 2, 2018.

[224] G. Kostovski, P. R. Stoddart, and A. Mitchell, "The optical fiber tip: an inherently light-coupled microscopic platform for micro- and nanotechnologies," *Adv. Mater.*, vol. 26, no. 23, pp. 3798–3820, 2014.

[225] W. S. Wong and A. Salleo, *Flexible electronics: materials and applications*, vol. 11. Springer Science & Business Media, 2009.

[226] A. Carlson, A. M. Bowen, Y. Huang, R. G. Nuzzo, and J. A. Rogers, "Transfer printing techniques for materials assembly and micro/nanodevice fabrication," *Adv. Mater.*, vol. 24, no. 39, pp. 5284–5318, 2012.

[227] K. J. Yu, Z. Yan, M. Han, and J. A. Rogers, "Inorganic semiconducting materials for flexible and stretchable electronics," *NPJ Flex. Electron.*, vol. 1, no. 1, p. 4, 2017.

[228] H. Yang, D. Zhao, S. Chuwongin, *et al*., "Transfer-printed stacked nanomembrane lasers on silicon," *Nat. Photonics*, vol. 6, no. 9, pp. 615–620, 2012.

[229] W. Zhou, Z. Ma, H. Yang, *et al*., "Flexible photonic-crystal Fano filters based on transferred semiconductor nanomembranes," *J. Phys. D. Appl. Phys.*, vol. 42, no. 23, p. 234007, 2009.

[230] Y. Chen, H. Lin, J. Hu, and M. Li, "Heterogeneously integrated silicon photonics for the mid-infrared and spectroscopic sensing," *ACS Nano*, vol. 8, no. 7, pp. 6955–6961, 2014.

[231] Y. Chen, H. Li, and M. Li, "Flexible and tunable silicon photonic circuits on plastic substrates," *Sci. Rep.*, vol. 2, p. 622, 2012.

[232] I. M. Pryce, K. Aydin, Y. A. Kelaita, R. M. Briggs, and H. A. Atwater, "Highly strained compliant optical metamaterials with large frequency tunability," *Nano Lett.*, vol. 10, no. 10, pp. 4222–4227, 2010.

[233] F. Laible, D. A. Gollmer, S. Dickreuter, D. P. Kern, and M. Fleischer, "Continuous reversible tuning of the gap size and plasmonic coupling of bow tie nanoantennas on flexible substrates," *Nanoscale*, vol. 10, no. 31, pp. 14915–14922, 2018.

[234] L. Zhu, J. Kapraun, J. Ferrara, and C. J. Chang-Hasnain, "Flexible photonic metastructures for tunable coloration," *Optica*, vol. 2, no. 3, pp. 255–258, 2015.

[235] X. Xu, H. Subbaraman, A. Hosseini, C.-Y. Lin, D. Kwong, and R. T. Chen, "Stamp printing of silicon-nanomembrane-based photonic devices onto flexible substrates with a suspended configuration," *Opt. Lett.*, vol. 37, no. 6, pp. 1020–1022, 2012.

[236] D. Chanda, K. Shigeta, S. Gupta, *et al*., "Large-area flexible 3D optical negative index metamaterial formed by nanotransfer printing," *Nat. Nanotechnol.*, vol. 6, p. 402, 2011.

[237] S. C. Malek, H.-S. Ee, and R. Agarwal, "Strain multiplexed metasurface holograms on a stretchable substrate," *Nano Lett.*, vol. 17, no. 6, pp. 3641–3645, 2017.

[238] P. Gutruf, C. Zou, W. Withayachumnankul, M. Bhaskaran, S. Sriram, and C. Fumeaux, "Mechanically tunable dielectric resonator metasurfaces at visible frequencies," *ACS Nano*, vol. 10, no. 1, pp. 133–141, 2016.

[239] X. Xu, B. Peng, D. Li, *et al*., "Flexible visible–infrared metamaterials and their applications in highly sensitive chemical and biological sensing," *Nano Lett.*, vol. 11, no. 8, pp. 3232–3238, 2011.

[240] A. Di Falco, Y. Zhao, and A. Alú, "Optical metasurfaces with robust angular response on flexible substrates," *Appl. Phys. Lett.*, vol. 99, no. 16, p. 163110, 2011.

[241] J. Burch, D. Wen, X. Chen, and A. Di Falco, "Conformable holographic metasurfaces," *Sci. Rep*., vol. 7, no. 1, p. 4520, 2017.

[242] F. Andrea Di, P. Martin, and F. K. Thomas, "Flexible metamaterials at visible wavelengths," *New J. Phys.*, vol. 12, no. 11, p. 113006, 2010.

[243] P.-C. Li and E. T. Yu, "Flexible, low-loss, large-area, wide-angle, wavelength-selective plasmonic multilayer metasurface," *J. Appl. Phys.*, vol. 114, no. 13, p. 133104, 2013.

[244] N. Sharac, H. Sharma, M. Veysi, *et al*., "Tunable optical response of bowtie nanoantenna arrays on thermoplastic substrates," *Nanotechnology*, vol. 27, no. 10, p. 105302, 2016.

[245] G. Zhang, C. Lan, H. Bian, R. Gao, and J. Zhou, "Flexible, all-dielectric metasurface fabricated via nanosphere lithography and its applications in sensing," *Opt. Express*, vol. 25, no. 18, pp. 22038–22045, 2017.

[246] M. Kahraman, P. Daggumati, O. Kurtulus, E. Seker, and S. Wachsmann-Hogiu, "Fabrication and characterization of flexible and tunable plasmonic nanostructures," *Sci. Rep.*, vol. 3, p. 3396, 2013.

[247] J. Y. Kim, H. Kim, B. H. Kim, *et al*., "Highly tunable refractive index visible-light metasurface from block copolymer self-assembly," *Nat. Commun.*, vol. 7, p. 12911, 2016.

[248] S. Aksu, M. Huang, A. Artar, *et al*., "Flexible plasmonics: flexible plasmonics on unconventional and nonplanar substrates," *Adv. Mater.*, vol. 23, no. 38, p. 4421, 2011.

[249] O. Vazquez-Mena, T. Sannomiya, M. Tosun, *et al*., "High-resolution resistless nanopatterning on polymer and flexible substrates for plasmonic biosensing using stencil masks," *ACS Nano*, vol. 6, no. 6, pp. 5474–5481, 2012.

[250] S. Aksu, A. A. Yanik, R. Adato, A. Artar, M. Huang, and H. Altug, "Nanostencil lithography for high-throughput fabrication of infrared plasmonic sensors," in *SPIE Defense, Security, and Sensing*, 2011, vol. 8031, p. 5.

[251] R. Hokari, K. Kurihara, N. Takada, and H. Hiroshima, "Development of simple high-resolution embedded printing for transparent metal grid conductors," *Appl. Phys. Lett.*, vol. 111, no. 6, p. 63107, 2017.

[252] R. Hokari, K. Kurihara, N. Takada, and H. Hiroshima, "Printed optical metamaterials composed of embedded silver nanoparticles for flexible applications," *Opt. Express*, vol. 26, no. 8, pp. 10326–10338, 2018.

[253] L. Duempelmann, J. A. Müller, F. Lütolf, B. Gallinet, R. Ferrini, and L. Novotny, "Controlling the color of plasmonic substrates with inkjet printing," *Adv. Opt. Mater.*, vol. 5, no. 17, p. 1700153, 2017.

[254] L. Fan, L. T. Varghese, Y. Xuan, J. Wang, B. Niu, and M. Qi, "Direct fabrication of silicon photonic devices on a flexible platform and its application for strain sensing," *Opt. Express*, vol. 20, no. 18, pp. 20564–20575, 2012.

[255] R. Madaka, V. Kanneboina, and P. Agarwal, "Low-temperature growth of amorphous silicon films and direct fabrication of solar cells on flexible polyimide and photo-paper substrates," *J. Electron. Mater.*, vol. 47, no. 8, pp. 4710–4720, 2018.

[256] Z. Shao, Y. Chen, H. Chen, *et al*., "Ultra-low temperature silicon nitride photonic integration platform," *Opt. Express*, vol. 24, no. 3, pp. 1865–1872, 2016.

[257] L. Li, P. Zhang, W.-M. Wang, *et al*., "Foldable and cytocompatible sol-gel TiO_2 photonics," *Sci. Rep.*, vol. 5, 2015.

[258] L. Li, H. Lin, S. Geiger, *et al*., "Amorphous thin films for mechanically flexible, multimaterial integrated photonics," *Am. Ceram. Soc. Bull*., vol. 95, no. 4, pp. 34–36, 2016.

[259] L. Li, Y. Zou, H. Lin, *et al*., "A fully-integrated flexible photonic platform for chip-to-chip optical interconnects," *J. Light. Technol.*, vol. 31, no. 24, pp. 4080–4086, 2013.

[260] R. G. DeCorby, N. Ponnampalam, H. T. Nguyen, and T. J. Clement, "Robust and flexible free-standing all-dielectric omnidirectional reflectors," *Adv. Mater.*, vol. 19, no. 2, pp. 193–196, 2007.

[261] J. D. Musgraves, N. Carlie, J. Hu, *et al*., "Comparison of the optical, thermal and structural properties of Ge-Sb-S thin films deposited using thermal evaporation and pulsed laser deposition techniques," *Acta Mater.*, vol. 59, no. 12, pp. 5032–5039, 2011.

[262] N. Carlie, J. D. Musgraves, B. Zdyrko, *et al*., "Integrated chalcogenide waveguide resonators for mid-IR sensing: leveraging material properties to meet fabrication challenges," *Opt. Express*, vol. 18, no. 25, pp. 26728–26743, 2010.

[263] J. Hu, V. Tarasov, N. Carlie, *et al*., "Exploration of waveguide fabrication from thermally evaporated Ge–Sb–S glass films," *Opt. Mater. (Amst).*, vol. 30, no. 10, pp. 1560–1566, 2008.

[264] J. Hu, N. N. Feng, N. Carlie, *et al*., "Optical loss reduction in high-index-contrast chalcogenide glass waveguides via thermal reflow," *Opt. Express*, vol. 18, no. 2, p. 1469, 2010.

[265] L. Petit, N. Carlie, B. Zdyrko, *et al.*, "Development of novel integrated bio/chemical sensor systems using chalcogenide glass materials," in *2nd International Symposium on Transparent Conducting Oxides*, vol. 6, no. 9, pp. 799–815, 2009.

[266] Y. Zou, H. Lin, O. Ogbuu, *et al*., "Effect of annealing conditions on the physio-chemical properties of spin-coated As_2Se_3 chalcogenide glass films," *Opt. Mater. Express*, vol. 2, no. 12, pp. 1723–1732, 2012.

[267] S. Novak, P. T. Lin, C. Li, *et al*., "Electrospray deposition of uniform thickness Ge23Sb7S70 and As40S60 chalcogenide glass films," *Jove-Journal Vis. Exp*., no. 114, 2016.

[268] Y. L. Zha, M. Waldmann, and C. B. Arnold, "A review on solution processing of chalcogenide glasses for optical components," *Opt. Mater. Express*, vol. 3, no. 9, pp. 1259–1272, 2013.

[269] Y. Zou, D. Zhang, H. Lin, *et al*., "High-performance, high-index-contrast chalcogenide glass photonics on silicon and unconventional non-planar substrates," *Adv. Opt. Mater.*, vol. 2, no. 5, pp. 478–486, 2014.

[270] M. V Kunnavakkam, F. M. Houlihan, M. Schlax, *et al*., "Low-cost, low-loss microlens arrays fabricated by soft-lithography replication process," *Appl. Phys. Lett.*, vol. 82, no. 8, pp. 1152–1154, 2003.

[271] W. Chen, R. H. W. Lam, and J. Fu, "Photolithographic surface micromachining of polydimethylsiloxane (PDMS)," *Lab Chip*, vol. 12, no. 2, pp. 391–395, 2012.

[272] L. Li, H. Lin, J. Michon, *et al*., "A new twist on glass: a brittle material enabling flexible integrated photonics," *Int. J. Appl. Glas. Sci.*, vol. 8, no. 1, pp. 61–68, 2017.

[273] J.-Y. Sun, N. Lu, J. Yoon, K.-H. Oh, Z. Suo, and J. J. Vlassak, "Inorganic islands on a highly stretchable polyimide substrate," *J. Mater. Res.*, vol. 24, no. 11, pp. 3338–3342, 2009.

[274] J. A. Rogers, T. Someya, and Y. Huang, "Materials and mechanics for stretchable electronics," *Science*, vol. 327, no. 5973, pp. 1603–1607, 2010.

[275] D.-H. Kim, R. Ghaffari, N. Lu, and J. A. Rogers, "Flexible and stretchable electronics for biointegrated devices," *Annu. Rev. Biomed. Eng.*, vol. 14, pp. 113–128, 2012.

[276] D. Qin, Y. Xia, and G. M. Whitesides, "Soft lithography for micro- and nanoscale patterning," *Nat. Protoc.*, vol. 5, p. 491, 2010.

[277] W. Li, H. Ge, W. Wu, *et al*., "Hybrid nanoimprint−soft lithography with sub-15 nm resolution," *Nano Lett.*, vol. 9, no. 6, pp. 2306–2310, 2009.

[278] K. E. Paul, M. Prentiss, and G. M. Whitesides, "Patterning spherical surfaces at the two-hundred-nanometer scale using soft lithography," *Adv. Funct. Mater.*, vol. 13, no. 4, pp. 259–263, 2003.

[279] R. J. Jackman, J. L. Wilbur, and G. M. Whitesides, "Fabrication of submicrometer features on curved substrates by microcontact printing," *Science*, vol. 269, no. 5224, pp. 664–666, 1995.

[280] D. Zhang, W. Yu, T. Wang, Z. Lu, and Q. Sun, "Fabrication of diffractive optical elements on 3-D curved surfaces by capillary force lithography," *Opt. Express*, vol. 18, no. 14, pp. 15009–15016, 2010.

[281] K. Thomas, H. Lukas, B. Iris, and M. Michael, "Nanoimprint lithography on curved surfaces prepared by fused deposition modelling," *Surf. Topogr. Metrol. Prop.*, vol. 3, no. 2, p. 24003, 2015.

[282] B. Farshchian, A. Amirsadeghi, S. M. Hurst, J. Wu, J. Lee, and S. Park, "Soft UV-nanoimprint lithography on non-planar surfaces," *Microelectron. Eng.*, vol. 88, no. 11, pp. 3287–3292, 2011.

[283] B. Li, J. Zhang, and H. Ge, "A sandwiched flexible polymer mold for control of particle-induced defects in nanoimprint lithography," *Appl. Phys. A*, vol. 110, no. 1, pp. 123–128, 2013.

[284] A. M. Bowen and R. G. Nuzzo, "Fabrication of flexible binary amplitude masks for patterning on highly curved surfaces," *Adv. Funct. Mater.*, vol. 19, no. 20, pp. 3243–3253, 2009.

[285] H. Huan, Y. Junghoon, M. Glennys, C. Yaofeng, A. S. Mark, and P. K. William, "Nano-fabrication with a flexible array of nano-apertures," *Nanotechnology*, vol. 23, no. 17, p. 175303, 2012.

[286] J. G. Kim, N. Takama, B. J. Kim, and H. Fujita, "Optical-softlithographic technology for patterning on curved surfaces," *J. Micromechanics Microengineering*, vol. 19, no. 5, p. 55017, 2009.

[287] J. Park, H. Fujita, and B. Kim, "Fabrication of metallic microstructure on curved substrate by optical soft lithography and copper electroplating," *Sensors Actuators A Phys.*, vol. 168, no. 1, pp. 105–111, 2011.

[288] A. M. Bowen, J. A. Ritchey, J. S. Moore, and R. G. Nuzzo, "Programmable chemical gradient patterns by soft grayscale lithography," *Small*, vol. 7, no. 23, pp. 3350–3362, 2011.

[289] M. Duocastella and C. B. Arnold, "Enhanced depth of field laser processing using an ultra-high-speed axial scanner," *Appl. Phys. Lett.*, vol. 102, no. 6, p. 061113, 2013.

[290] D. Radtke and U. D. Zeitner, "Laser-lithography on non-planar surfaces," *Opt. Express*, vol. 15, no. 3, pp. 1167–1174, 2007.

[291] M. Duocastella and C. B. Arnold, "Bessel and annular beams for materials processing," *Laser Photon. Rev.*, vol. 6, no. 5, pp. 607–621, 2012.

[292] P. Mouroulis, D. W. Wilson, P. D. Maker, and R. E. Muller, "Convex grating types for concentric imaging spectrometers," *Appl. Opt.*, vol. 37, no. 31, pp. 7200–7208, 1998.

[293] J. Zhang, B. Shokouhi, and B. Cui, "Tilted nanostructure fabrication by electron beam lithography," *J. Vac. Sci. Technol. B*, vol. 30, no. 6, p. 06F302, 2012.

[294] F. Ranveig, A. Akshay, H. Richard, M. G. Martin, H. Bodil, and K. B. Karl, "Exploring proximity effects and large depth of field in helium ion beam lithography: large-area dense patterns and tilted surface exposure," *Nanotechnology*, vol. 29, no. 27, p. 275301, 2018.

[295] J. Chang, Q. Zhou, and A. Zettl, "Facile electron-beam lithography technique for irregular and fragile substrates," *Appl. Phys. Lett.*, vol. 105, no. 17, p. 173109, 2014.

[296] J. Linden, C. Thanner, B. Schaaf, S. Wolff, B. Lägel, and E. Oesterschulze, "Spray coating of PMMA for pattern transfer via electron beam lithography on surfaces with high topography," *Microelectron. Eng.*, vol. 88, no. 8, pp. 2030–2032, 2011.

[297] J. Zhang, C. Con, and B. Cui, "Electron beam lithography on irregular surfaces using an evaporated resist," *ACS Nano*, vol. 8, no. 4, pp. 3483–3489, 2014.

[298] C. Con, J. Zhang, and B. Cui, "Nanofabrication of high aspect ratio structures using an evaporated resist containing metal," *Nanotechnology*, vol. 25, no. 17, 2014.

[299] P. W. Leech, N. Wu, and Y. Zhu, "Application of dry film resist in the fabrication of microfluidic chips for droplet generation," *J. Micromechanics Microengineering*, vol. 19, no. 6, p. 65019, 2009.

[300] L. Duanhui, L. Lan, J. Bradley, *et al*., "Wafer integrated micro-scale concentrating photovoltaics," *Prog. Photovoltaics Res. Appl.*, vol. 26, no. 8, pp. 651–658, 2018.

[301] R. H. Pedersen, M. Hamzah, S. Thoms, P. Roach, M. R. Alexander, and N. Gadegaard, "Electron beam lithography using plasma polymerized hexane as resist," *Microelectron. Eng.*, vol. 87, no. 5, pp. 1112–1114, 2010.

[302] I. R. Peterson, "Langmuir–Blodgett electron-beam resists," *IEE Proc. I - Solid-State Electron Devices*, vol. 130, no. 5, pp. 252–255, 1983.

[303] G. M. King, G. Schürmann, D. Branton, and J. A. Golovchenko, "Nanometer patterning with ice," *Nano Lett.*, vol. 5, no. 6, pp. 1157–1160, 2005.

[304] P. Ruchhoeft and J. C. Wolfe, "Optimal strategy for controlling linewidth on spherical focal surface arrays," *J. Vac. Sci. Technol. B*, vol. 18, no. 6, pp. 3185–3189, 2000.

[305] P. Ruchhoeft, M. Colburn, B. J. Choi, *et al*., "Patterning curved surfaces: template generation by ion beam proximity lithography and relief transfer by step and flash imprint lithography," *J. Vac. Sci. Technol. B*, vol. 17, no. 6, pp. 2965–2969, 1999.

[306] D. Parikh, B. Craver, H. N. Nounu, F. O. Fong, and J. C. Wolfe, "Nanoscale pattern definition on nonplanar surfaces using ion beam proximity lithography and conformal plasma-deposited resist," *J. Microelectromechanical Syst.*, vol. 17, no. 3, pp. 735–740, 2008.

[307] A. Ricciardi, A. Crescitelli, P. Vaiano, *et al*., "Lab-on-fiber technology: a new vision for chemical and biological sensing," *Analyst*, vol. 140, no. 24, pp. 8068–8079, 2015.

[308] E. J. Smythe, M. D. Dickey, J. Bao, G. M. Whitesides, and F. Capasso, "Optical antenna arrays on a fiber facet for in situ surface-enhanced Raman scattering detection," *Nano Lett.*, vol. 9, no. 3, pp. 1132–1138, 2009.

[309] D. J. Lipomi, R. V. Martinez, M. A. Kats, *et al*., "Patterning the tips of optical fibers with metallic nanostructures using nanoskiving," *Nano Lett.*, vol. 11, no. 2, pp. 632–636, 2010.

[310] P. Jia and J. Yang, "Integration of large-area metallic nanohole arrays with multimode optical fibers for surface plasmon resonance sensing," *Appl. Phys. Lett.*, vol. 102, no. 24, p. 243107, 2013.

[311] X. Zhang, F. Liu, and Y. Lin, "Direct transfer of metallic photonic structures onto end facets of optical fibers," *Front. Phys*., vol. 4, p. 31, 2016.

[312] G. Shambat, J. Provine, K. Rivoire, T. Sarmiento, J. Harris, and J. Vučković, "Optical fiber tips functionalized with semiconductor photonic crystal cavities," *Appl. Phys. Lett.*, vol. 99, no. 19, p. 191102, 2011.

[313] I. W. Jung, B. Park, J. Provine, R. T. Howe, and O. Solgaard, "Highly sensitive monolithic silicon photonic crystal fiber tip sensor for simultaneous measurement of refractive index and temperature," *J. Light. Technol.*, vol. 29, no. 9, pp. 1367–1374, 2011.

[314] B. Wang, T. Siahaan, Dündar, *et al*., "Photonic crystal cavity on optical fiber facet for refractive index sensing," *Opt. Lett.*, vol. 37, no. 5, pp. 833–835, 2012.

[315] M. Boerkamp, Y. Lu, J. Mink, Ž. Zobenica, and R. W. van der Heijden, "Multiple modes of a photonic crystal cavity on a fiber tip for multiple parameter sensing," *J. Light. Technol.*, vol. 33, no. 18, pp. 3901–3906, 2015.

[316] L. Li, I. Bayn, M. Lu, *et al*., "Nanofabrication on unconventional substrates using transferred hard masks," *Sci. Rep.*, vol. 5, p. 7802, 2015.

[317] C. L. Arce, K. De Vos, T. Claes, K. Komorowska, D. Van Thourhout, and P. Bienstman, "Silicon-on-insulator microring resonator sensor integrated on an optical fiber facet," *IEEE Photonics Technol. Lett.*, vol. 23, no. 13, pp. 890–892, 2011.

[318] M. Pisco, F. Galeotti, G. Quero, *et al*., "Nanosphere lithography for optical fiber tip nanoprobes," *Light. Appl.*, vol. 6, 2017.

[319] P. Di Palma, C. Taddei, A. Borriello, *et al*., "Self-assembled colloidal photonic crystal on the fiber optic tip as a sensing probe," *IEEE Photonics J.*, vol. 9, no. 2, 2017.

[320] Q. Giuseppe, Z. Gianluigi, Managò Stefano, *et al*., "Nanosphere lithography on fiber: towards engineered lab-on-fiber SERS optrodes," *Sensors*, vol. 18, no. 3, 2018.

[321] R. Bachelot, C. Ecoffet, D. Deloeil, P. Royer, and D. J. Lougnot, "Integration of micrometer-sized polymer elements at the end of optical fibers by free-radical photopolymerization," *Appl. Opt.*, vol. 40, no. 32, pp. 5860–5871, 2001.

[322] P. S. Kelkar and J. Beauvais, "Nano patterning on optical fiber and laser diode facet with dry resist," *J. Vac. Sci. Technol. A*, vol. 22, no. 3, pp. 743–746, 2004.

[323] M. Prasciolu, D. Cojoc, S. Cabrini, *et al*., "Design and fabrication of on-fiber diffractive elements for fiber-waveguide coupling by means of e-beam lithography," *Microelectron. Eng.*, vol. 67–8, pp. 169–174, 2003.

[324] N. Wang, M. Zeisberger, U. Hubner, and M. A. Schmidt, "Nanotrimer enhanced optical fiber tips implemented by electron beam lithography," *Opt. Mater. Express*, vol. 8, no. 8, pp. 2246–2255, 2018.

[325] V. M. Sundaram and S. B. Wen, "Fabrication of micro-optical devices at the end of a multimode optical fiber with negative tone lift-off EBL," *J. Micromechanics Microengineering*, vol. 22, no. 12, 2012.

[326] J. B. Kim and K. H. Jeong, "Batch fabrication of functional optical elements on a fiber facet using DMD based maskless lithography," *Opt. Express*, vol. 25, no. 14, pp. 16854–16859, 2017.

[327] Y. B. Lin, J. P. Guo, and R. G. Lindquist, "Demonstration of an ultra-wideband optical fiber inline polarizer with metal nano-grid on the fiber tip," *Opt. Express*, vol. 17, no. 20, pp. 17849–17854, 2009.

[328] J. J. Kaufman, E. H. Banaei, A. F. Abouraddy, and Ieee, "Inscription of photonic devices on the tip of a chalcogenide glass fiber," in *Conference on Lasers and Electro-Optics (CLEO)*, 2012.

[329] S. F. Feng, X. P. Zhang, H. Wang, M. D. Xin, and Z. Z. Lu, "Fiber coupled waveguide grating structures," *Appl. Phys. Lett.*, vol. 96, no. 13, 2010.

[330] H. Hemmati, Y. H. Ko, and R. Magnusson, "Fiber-facet-integrated guided-mode resonance filters and sensors: experimental realization," *Opt. Lett.*, vol. 43, no. 3, pp. 358–361, 2018.

[331] E. G. Johnson, J. Stack, T. J. Suleski, C. Koehler, and W. Delaney, "Fabrication of micro optics on coreless fiber segments," *Appl. Opt.*, vol. 42, no. 5, pp. 785–791, 2003.

[332] G. Kostovski, D. J. White, A. Mitchell, M. W. Austin, and P. R. Stoddart, "Nanoimprinted optical fibres: biotemplated nanostructures for SERS sensing," *Biosens. Bioelectron.*, vol. 24, no. 5, pp. 1531–1535, 2009.

[333] G. Calafiore, A. Koshelev, F. I. Allen, *et al*., "Nanoimprint of a 3D structure on an optical fiber for light wavefront manipulation," *Nanotechnology*, vol. 27, no. 37, p. 375301, 2016.

[334] S. Tabassum, Y. Wang, J. Qu, *et al*., "Patterning of nanophotonic structures at optical fiber tip for refractive index sensing," in *SENSORS, 2016 IEEE*, 2016, pp. 1–3.

[335] J. Viheriala, T. Niemi, J. Kontio, T. Rytkonen, and M. Pessa, "Fabrication of surface reliefs on facets of singlemode optical fibres using nanoimprint lithography," *Electron. Lett.*, vol. 43, no. 3, pp. 150–151, 2007.

[336] G. Calafiore, A. Koshelev, T. P. Darlington, *et al*., "Campanile near-field probes fabricated by nanoimprint lithography on the facet of an optical fiber," *Sci. Rep.*, vol. 7, no. 1, p. 1651, 2017.

[337] G. Kostovski, U. Chinnasamy, S. Jayawardhana, P. R. Stoddart, and A. Mitchell, "Sub-15nm optical fiber nanoimprint lithography: a parallel, self-aligned and portable approach," *Adv. Mater.*, vol. 23, no. 4, pp. 531–535, 2011.

[338] S. Scheerlinck, D. Taillaert, D. Van Thourhout, and R. Baets, "Flexible metal grating based optical fiber probe for photonic integrated circuits," *Appl. Phys. Lett.*, vol. 92, no. 3, p. 31104, 2008.

[339] S. Pilevar, K. Edinger, W. Atia, I. Smolyaninov, and C. Davis, "Focused ion-beam fabrication of fiber probes with well-defined apertures for use in near-field scanning optical microscopy," *Appl. Phys. Lett.*, vol. 72, no. 24, pp. 3133–3135, 1998.

[340] A. Dhawan, J. F. Muth, D. N. Leonard, *et al*., "Focused ion beam fabrication of metallic nanostructures on end faces of optical fibers for chemical sensing applications," *J. Vac. Sci. Technol. B Microelectron. Nanom. Struct. Process. Meas. Phenom*., vol. 26, no. 6, pp. 2168–2173, 2008.

[341] M. Principe, M. Consales, A. Micco, *et al*., "Optical fiber meta-tips," *Light Sci. Appl.*, vol. 6, no. 3, p. e16226, 2017.

[342] F. Schiappelli, R. Kumar, M. Prasciolu, *et al*., "Efficient fiber-to-waveguide coupling by a lens on the end of the optical fiber fabricated by focused ion beam milling," *Microelectron. Eng.*, vol. 73, pp. 397–404, 2004.

[343] C. Ma and A. Wang, "Optical fiber tip acoustic resonator for hydrogen sensing," *Opt. Lett.*, vol. 35, no. 12, pp. 2043–2045, 2010.

[344] F. Wang, W. Yuan, O. Hansen, and O. Bang, "Selective filling of photonic crystal fibers using focused ion beam milled microchannels," *Opt. Express*, vol. 19, no. 18, pp. 17585–17590, 2011.

[345] A. Micco, A. Ricciardi, M. Pisco, V. La Ferrara, and A. Cusano, "Optical fiber tip templating using direct focused ion beam milling," *Sci. Rep.*, vol. 5, p. 15935, 2015.

[346] Y. Fu and N. K. A. Bryan, "Investigation of physical properties of quartz after focused ion beam bombardment," *Appl. Phys. B*, vol. 80, no. 4–5, pp. 581–585, 2005.

[347] H. Lin, L. Li, F. Deng, *et al*., "Demonstration of mid-infrared waveguide photonic crystal cavities," *Opt. Lett.*, vol. 38, no. 15, pp. 2779–2782, 2013.

[348] J. F. Xing, X. Z. Dong, W. Q. Chen, *et al*., "Improving spatial resolution of two-photon microfabrication by using photoinitiator with high initiating efficiency," *Appl. Phys. Lett.*, vol. 90, no. 13, p. 131106, 2007.